論文 / 著書情報
Article / Book Information

Title	GAN-driven discovery of low-cost non-noble metallic electrocatalysts for glycerol electroreduction
Authors	Muhammad Harussani Moklis, Cries Avian, Cheng Shuo, Sasipa Boonyubol, Jenq-Shiou Leu, Koichi Mikami, Jeffrey S. Cross
Citation	Electrochimica Acta, Vol. 539, , p. 147096
Pub. date	2025, 8
DOI	https://dx.doi.org/10.1016/j.electacta.2025.147096
Creative Commons	Information is in the article.

Electrochimica Acta 539 (2025) 147096

Contents lists available at ScienceDirect

Electrochimica Acta

journal homepage: www.journals.elsevier.com/electrochimica-acta

GAN-driven discovery of low-cost non-noble metallic electrocatalysts for glycerol electroreduction

Muhammad Harussani Moklis [a,*], Cries Avian [b,c], Cheng Shuo [a], Sasipa Boonyubol [a], Jenq-Shiou Leu [b], Koichi Mikami [a], Jeffrey S. Cross [a]

[a] Energy Science and Engineering, Department of Transdisciplinary Science and Engineering, Institute of Science Tokyo, 2-12-1, Ookayama, Meguro-ku, Tokyo 152-8550, Japan
[b] Department of Electronic and Computer Engineering, National Taiwan University of Science and Technology, Taipei 106, Taiwan
[c] Department of Electrical Engineering, Universitas Brawijaya, Malang, Jawa Timur 65145, Indonesia

ARTICLE INFO

Keywords:
Elemental screening
Metallic compounds
Electrocatalyst
Non-noble catalyst
Generative adversarial networks

ABSTRACT

Glycerol, a major by-product generated in abundance during biodiesel production, presents a valuable opportunity for conversion into high-value chemicals through electrochemical processes. One of the main challenges in advancing glycerol electroreduction is the inefficiency of current electrocatalyst discovery methods to recognize materials tailored for specific cathodic reaction. Conventional trial-and-error approaches struggle to efficiently navigate the vast chemical design space for optimizing electrocatalyst properties. Here, we employ a generative adversarial network (GAN) to discover new hypothetical low-cost non-noble metallic electrocatalysts favoring cathodic reactions in glycerol electrocatalytic reduction (ECR). Trained on a curated dataset of over 5000 thermodynamically stable mono-, bi-, and trimetallic compounds from the Materials Project (MP) database, our GAN architecture generates 400,000 hypothetical candidates not existing in the training dataset with a uniqueness of 99.94 %, while adhering to chemical validity, thermodynamic feasibility, and electrochemical property constraints. Notably, the GAN learns implicit chemical rules despite no explicit enforcement, producing chemically valid material compositions. Further conditional screening identifies 18 top candidates, with metallic compounds significantly outnumbering metallic oxides–highlighting the natural favorability of metallic systems for electroreduction. Among the top candidates, Co-Zr-X (X = Ba, Ti) trimetallics emerge, exhibiting promise for suppressing hydrogen evolution reaction (HER) and enhancing selective glycerol ECR. These findings underscore the potential of GAN-based generative design in accelerating electrocatalyst discovery, offering a data-driven pathway to sustainable biodiesel by-product utilization.

1. Introduction

The surge in biodiesel production has resulted in an overproduction of crude glycerol [1], a major by-product with a negative market value of –165 USD per tonne [2] and a projected global output of about 6.3 million tonnes by 2025 [3]. Electrochemical reduction (ECR) has emerged as a promising route for valorizing this by-product into valuable chemicals such as 1,2-propanediol, glyceric acid, and dihydroxyacetone [4–6]. However, large-scale implementation of this technology critically hinges on optimizing key process parameters–particularly developing advanced electrocatalysts [7], that highly reactive, stable, and cost-effective–an ongoing challenge that remain unresolved by conventional catalyst design paradigms. To date, ECR systems have predominantly employed noble metal-based cathodic catalysts, mainly platinum (Pt), palladium (Pd), gold (Au), etc., long regarded as benchmark catalytic materials for electrochemical reactions [8,9]. However, these catalysts are costly and have shown its underperformance in glycerol ECR, primarily due to competitive parasitic hydrogen evolution reaction (HER), which reduces faradaic efficiency by up to 40 % [10]. While alternative electrocatalysts–including monometallics [11], carbon-based composites [12,13], and bimetallic alloys [14]–have been explored to overcome the limitations of noble metals, their discovery still largely relies on empirical, trial-and-error experimentation. This conventional approach is often slow, resource-intensive, and lacks a fundamental understanding of the underlying structure–property relationships that govern electrocatalytic performance. As a result,

* Corresponding author.
E-mail address: harussani.m.ab@m.titech.ac.jp (M.H. Moklis).

https://doi.org/10.1016/j.electacta.2025.147096
Received 15 July 2025; Received in revised form 28 July 2025; Accepted 4 August 2025
Available online 5 August 2025

promising material candidates may be overlooked, and the optimization of catalyst compositions remains inefficient and non-systematic.

This gap is exacerbated by the combinatorial explosion of possible compositions inherent to multi-metallic systems–exceeding 10^4 combinations for bimetallics and 10^5 for trimetallics [15]. Such vast design spaces make exhaustive high-throughput screening infeasible. While brute-force molecular simulations or first-principles calculations have been applied [16–19], their computational cost limits exploration to only a small fraction of the possible composition space. More intelligent sampling methods are required–approaches that employ explicit physicochemical knowledge, and also implicit elemental composition knowledge embodied within known synthesized materials. This has spurred interest in generative machine learning (ML) approaches, particularly autoencoder generative adversarial networks (AE-GAN), variational autoencoders (VAEs) and hybrid models (e.g., VAE-GANs) [20], offer a powerful alternative for addressing these challenges while accelerating the discovery and design of metallic materials. Among these approaches, VAEs are the most widely applied in materials generation, particularly for crystalline systems. They have demonstrated strong performance in property-conditioned design. For instance, Mal et al. [21] used a conditional VAE to predict formation energies (MAE = 0.162 eV/atom) and magnetization (MAE = 0.07 T), while Court et al. [22] achieved lattice parameter predictions with an MAE of 0.06 Å and screened 12,000 structures in 12 h using a single GPU. However, the latent-space regularization in VAEs can blur discrete atomic-scale features and stoichiometric constraints [23,24], which are essential in catalyst design. As a result, VAEs tend to favor averaged structures, potentially missing fine variations in surface terminations, defects, and compositional boundaries that are critical for catalytic performance, especially for HER suppression.

GANs, on the other hand, excel at generating structurally realistic and compositionally valid materials. By employing structured representations such as sequences or graphs, GANs capture the underlying rules governing valid chemical compositions and apply these learned patterns to generate realistic, chemically plausible compounds. Their adversarial training setup enables high-resolution feature learning and better preservation of discrete material constraints [25–27]. GANs have been widely applied in various fields such as in organic chemistry for drug discovery [28,29], screening inorganic materials [30,31], and crystal discovery [32]. Dan et al. [30] used a GAN trained on the Inorganic Crystal Structure Database (ICSD) to generate new crystal structures with an 84.5 % validity rate and over 92 % novelty, while Türk et al. [33] showed that GANs achieved higher coverage (up to 89 %) than VAEs (54–62 %) in elpasolite classification. However, GANs' performance across studies is less consistent: reported validity rates range from 66 % [33] to 84.5 % [30], compared to VAEs, which more consistently reach 83–89 % validity and up to 0.997 uniqueness [33,34]. These findings suggest that while VAEs offer stable and interpretable property prediction pipelines, GANs are more effective at capturing complex structural features needed for practical electrocatalyst design. Nouira et al. [32] had discovered crystalGAN trained on various databases such as ICSD and Open Quantum Materials Database (OQMD), successfully generated novel crystal structures. Jangid et al. [35] demonstrated GANs' ability to generate polycrystalline microstructures with fewer than 0.2 % nonphysical grains, while Yang et al. [36] used style-based GANs to optimize optical absorption by 4.8 %. These capabilities are crucial when modeling electrocatalysts, where defect structures, heterogeneous surfaces, and atomic-level morphologies critically influence reaction rates and selectivity.

Hybrid models such as VAE-GANs [37] attempt to merge VAE interpretability with GAN realism, but often introduce training complexity and may compromise GANs' structural fidelity. Given that electrocatalyst performance hinges on features such as surface site accessibility, lattice strain, and electron density distributions, GANs' ability to replicate realistic atomic-scale variations offers a distinct advantage. Additionally, the rich structural and electronic data from the Materials Project (MP) database makes it well suited for training GANs that can infer both global trends and local structural details. Despite these advantages, the application of GANs to multi-metallic electrocatalyst discovery remains largely unexplored.

Here, we bridge this gap by deploying an AE-GAN framework to discover low-cost, non-noble metallic electrocatalysts optimized for cathodic reaction in glycerol ECR, as illustrated in Fig. 1. This model is trained on a curated dataset of about 40,000 materials from the Materials Project (MP) and pymatgen databases, incorporating critical features such as formation energy, elemental electronegativity, and Fermi energy (E_{fermi}). By learning implicitly from the compositional rules embedded in known stable compounds, the GAN generates realistic hypothetical candidates that are more likely to exhibit desirable electrocatalytic behavior. This data-driven approach not only accelerates the discovery of electrocatalysts but also provides a generalizable framework for sustainable chemical synthesis, thereby increasing the economic viability and sustainability of biodiesel production.

2. Methodology

2.1. Datasets buildups

A subset of metallic materials was extracted from the MP database, containing their crystalline materials data, thermodynamics and electrochemical properties recorded via high-throughput density functional theory (DFT) calculations and experimental data, see Table S1. The dataset comprises 153,311 metallic compounds based on 98 metals and metalloids.

To tailor the dataset for electrocatalytic discovery, multi-stage screening protocol was designed to filter the raw data through three critical selection tiers. First, non-metallic compounds and high-entropy systems (>3 metal species) were excluded despite their potential synergistic effects, as they present several practical limitations: (1) indeterminate active sites that hinder reproducibility and mechanistic studies [38], (2) complex synthesis requiring non-equilibrium methods that are cost-prohibitive for scalable production [39–41], and (3) limited evidence in catalytic literature demonstrating superior glycerol ECR performance compared to simpler bi-/trimetallic systems [42–44]. Second, noble metals, lanthanides, actinides, and hazardous elements were also excluded due to their prohibitive costs and sustainability concerns. Finally, the remaining 41 metals were verified for economic viability using the Herfindahl-Hirschman Index (HHI) [45] via matminer to prioritize low-cost, abundant candidates. Thus, only mono-, bi-, and trimetallic compounds, along with their oxides, were retained. Detailed records for the extracted compounds were stated clearly in Table 1.

This rigorous selection process yielded two key datasets: (1) the MP Train dataset (38,183 mono-, bi- and trimetallic compounds) representing compositionally viable candidates of 41 metal elements, and (a) the MP_filter Train dataset (thermodynamically stable 4647 compounds) refined by thermodynamic stability filter built-in within the MP database–based on energy above hull and formation energy per atom. While this approach ensures practical feasibility, we acknowledge it may exclude potentially valuable metastable phases–a consideration addressed in our limitations section and targeted for future work.

2.2. GAN neutral networks training

A convolutional generative adversarial network was constructed from scratch comprising a generator (G) and a discriminator (D), as illustrated in Fig. 2. The generator adopts a staircase-like architecture composed of progressively expanding transposed convolutional layers. This design allows the network to gradually up-sample and refine latent noise vectors (Z) into structured material representations by incorporating increasingly complex spatial patterns at each layer. Such hierarchical generation is particularly suited for encoding compositional and

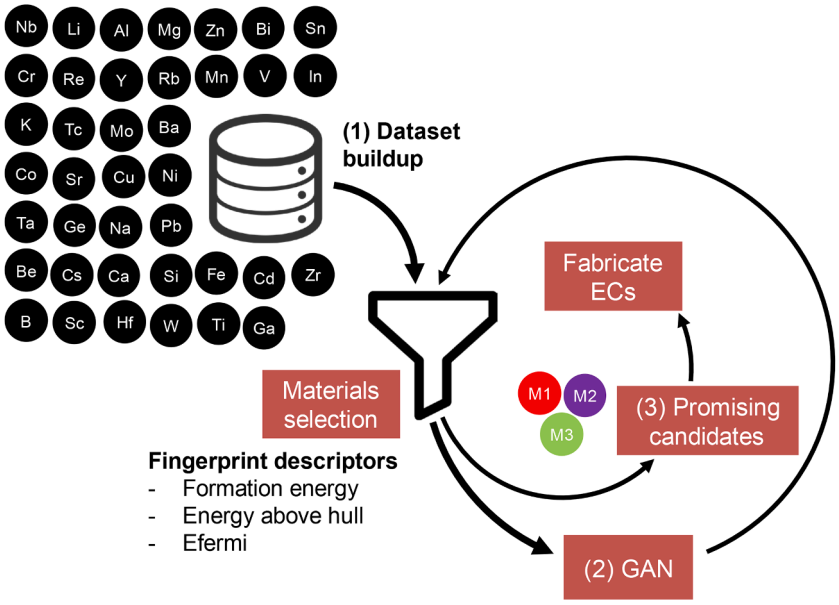

Fig. 1. Schematic diagram of how the computation works.

Table 1
Extraction of filtered and non-filtered data for mono-, bi-, and trimetallic materials.

Filter	Element amount	Sample amount					Dataset label
		Mono	Bi	Tri	Others	Total	
No filter	98	23,471	62,460	55,488	11,892	153,311	-
<=3 metals	98	23,471	62,460	55,488	-	141,419	-
Low-cost, <=3 metals	41	2426	15,497	20,260	-	38,183	MP
Stable, <=3 metals	98	4064	14,728	14,253	-	33,045	-
Stable, low-cost, <=3 metals	41	129	2090	2428	-	4647	MP_filter

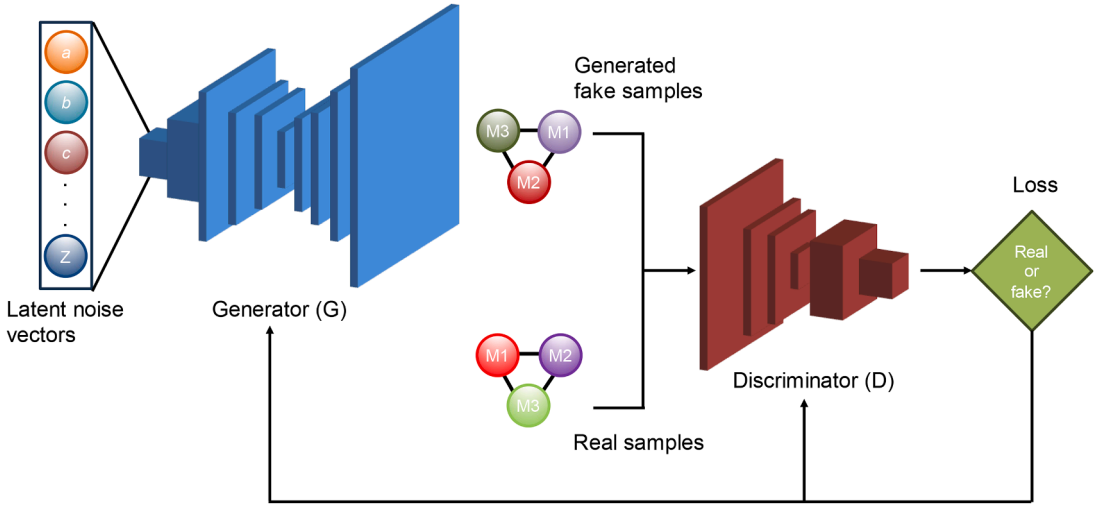

Fig. 2. GAN architecture for low-cost non-noble metallic electrocatalysts.

structural regularities often found in crystalline materials or catalytic motifs.

The discriminator was designed with an autoencoder-like structure, where input material candidates, either generated or real, are passed through a contracting convolutional encoder followed by a decoder that attempts to reconstruct the input. This approach is inspired by feature matching and reconstruction-based discrimination, where the network learns not only to distinguish real from fake inputs but also to reconstruct valid chemical and structural patterns. By embedding this autoencoding task, the discriminator provides richer gradients to the generator and helps stabilize training, especially in high-dimensional chemical spaces.

Both networks were optimized using the LeakyReLU activation function and trained for 100 epochs using a learning rate of 0.0002. Optimal hyperparameters (summarized in Table 2) were tuned empirically to ensure convergence and diversity in the generated candidates.

Table 2
The final optimum hyperparameters for GAN models trained.

Component	Hyperparameter	Optimized value
General	'latent_dim'	100
Learning rate	'initial_learning_rate'	0.0002
	'decay_steps'	1000
	'decay_rate'	0.99
	'staircase'	True
Generator	Layer sizes	512, 256, 128, 64, 128, 256, 512
	'activation'	LeakyReLU (alpha=0.2), ReLU (latent space), Tanh
	'momentum'	0.8
	'disc_loss'	'binary_crossentropy'
Discriminator	Layer sizes	256, 128, 1
	'activation'	LeakyReLU (alpha=0.2), Sigmoid
	'disc_loss'	'binary_crossentropy'

The framework was validated using 10-fold cross-validation, achieving consistent performance: mean absolute error (MAE) of 0.069 ± 0.006, mean squared error (MSE) of 0.081 ± 0.009, and root mean square error (RMSE) of 0.285 ± 0.017. Upon training completion, the GAN was used to generate 100,000 hypothetical electrocatalyst compositions, which were categorized into. MP_Generated (raw GAN outputs without post-screening), and MP_filter Generated (candidates filtered for stability and elemental feasibility).

2.3. Generated compound checks

In this study, rigorous three-tier chemical checks including validity check, uniqueness check and performance check were implemented, to ensure the generated materials are chemically plausible, structurally novel and functionally promising for glycerol ECR. Each check was designed to systematically filter out unstable, redundant, or catalytically inactive candidates, narrowing the selection to the most viable compounds for experimental synthesis.

2.3.1. Chemical validity check

Three chemical filters which includes charge neutrality (CN), electronegativity balance (EN) and crystal system (CS) validity were applied to the training and generated sets. CN check was enforced to eliminate unrealistic stoichiometries where ionic charges were unbalanced, as such compounds would be inherently unstable. Here, we applied a deep learning-based charge-neutrality predictor BERTOS [46]. EN check was then applied to ensure that the predicted bonds between elements were physically reasonable. According to Davies et al. [47], a stable compound should obey the relation of $\chi^{cation} < \chi^{anion}$ where the Pauling electronegativity scale was employed, which help reduces the allowed compositions. Whereas CS check, followed established methodologies from Hahn [48], performed to verify that the proposed atomic arrangements were compatible with known symmetry constraints, preventing nonsense or strained lattices. The percentages of materials within the training and generated datasets that obey these rules is calculated.

2.3.2. Uniqueness and novelty check

To check the uniqueness of the generated samples, the percentages of unique samples out of the number of all generated samples were calculated. Using structural, electrochemical and other descriptors fingerprinting, uniqueness was quantified by cross-referencing the generated dataset against known compounds in the original datasets. This step was crucial to avoid rediscovering known compounds or trivial variations of existing ones. Additionally, the distribution of the metallic combinations (mono-, bi-, and tri-metallic systems and their oxides) was analyzed to assess whether this GAN algorithm produced chemically diverse outputs or overrepresented certain compositions. Here, compounds with truly novel configurations were prioritized.

2.3.3. Descriptor-based performance check

This step evaluated whether the generated compounds possess electronic properties suitable for electrocatalytic reduction application. Two critical electrocatalytic features, such as E_{fermi} and band gaps, were extracted, both of which influence surface reactivity and electron transport. Compounds were screened based on literature-informed thresholds that favor efficient electron transfer and selective product formation under cathodic conditions. Their features were extracted and illustrated into a violin plot for comparisons.

2.3.4. Model consistency check

To assess the consistency and credibility of the GAN-generated outputs, their predicted properties were compared against independent ML models trained on experimentally and computationally derived datasets Specifically, two predictors–Magpie descriptors, constructed via the matminer package [49], to estimate average electronegativity, and ElemNet [50], a deep learning-based model for predicting formation energies–were implemented.

ElemNet [50] is a deep neural network that designed to predict materials properties using only elemental compositions as input. Unlike traditional ML models that rely on handcrafted physical descriptors, ElemNet learns chemical interactions directly from data, enabling it to generalize even to unseen chemical systems. It was pre-trained from scratch on large datasets like OQMD and fine-tuned using transfer learning for smaller DFT or experimental datasets. This enables it to generalize well, even to chemical systems not present in its training data, including predictions for phase stability and formation energy.

In our workflow, each GAN-generated compound was passed through ElemNet to predict its formation energy. Consistency was defined as a numerical agreement between the GAN and ElemNet predictions within a strict tolerance of ±0.1 eV per atom. For electronegativity, the Magpie-predicted average value served as a reference, and a compound was considered consistent if the GAN-generated value fell within the range defined by the Magpie mean ± average deviation. This comparative consistency check served as a secondary filter to reinforce the credibility of the GAN outputs and to identify candidates whose predicted properties reinforced by existing data-driven models.

2.4. Conditional screening for potential new candidates

A final conditional screening was applied to shortlist hypothetical materials with favorable profiles for glycerol ECR where all of them passed previous checks within Section 2.3. These top-performing candidates will be advanced to experimental validations as potential electrocatalysts for glycerol ECR, which were selected based on their three key descriptors derived from prior computational studies [51,52], which includes thermodynamic stability based on their formation energy per atom (≤0.0 eV), phase stability of energy above hull (≤0.0 eV), and electronic properties of E_{fermi} levels (>3.0 eV), potentially suppressing competing reactions like HER. Only compounds meeting all these criteria were selected as our best candidates for further application. This step narrowed down the search space to hypothetical materials that are not only chemically valid and novel but also meet key stability and electronic requirements relevant to electrocatalytic applications

2.5. Confirming stability with energy above hull calculations and phase diagram creation

To evaluate the phase stability of the top GAN-generated candidates, the energy above hull (E_{hull}) was calculated using a convex hull analysis based on Materials Project data. Formation energies predicted by the GAN were combined with elemental reference energies obtained via the Materials Project API. Each compound's total energy was calculated as Equation 1,

$$E_{total} = \left(E_f^{GAN} \times N_{atoms}\right) + \sum_i \left(n_i \times E_{ref,i}^{MP}\right) \quad (1)$$

where E_f^{GAN} is the GAN-predicted formation energy per atom, N_{atoms} is the total number of atoms in the formula unit, n_i is the number of atoms of element *i*, and $E_{ref,i}^{MP}$ is the reference energy per atom of element i from Materials Project. This total energy was then used to create a ComputedEntry, which was added to the set of known entries for that chemical system. Using pymatgen, the phase diagram was constructed with the PhaseDiagram class and computed each compound's energy above hull using get_e_above_hull().

Compounds with $E_{hull} \leq 0.05$ eV/atom were considered thermodynamically stable, while those within a moderate range (e.g., up to ~0.1 eV/atom) were classified as metastable and potentially synthesizable under non-equilibrium conditions. To support interpretation, phase diagrams were also plotted using the OQMD Phase Diagram Creation Tool, where GAN-generated compounds were visualized alongside known stable phases. This provided a graphical overview of each compound's position within its phase space and helped assess its likelihood of formation relative to competing phases.

This two-part stability check—numerical E_{hull} validation and visual phase diagram inspection—ensured that only the most thermodynamically viable candidates were selected for further application.

3. Results and discussion

3.1. The model performance of GANs

The GAN model was trained and evaluated using 23 selected features encompassing electronic, structural, and compositional descriptors to comprehensively learning the complex relationships governing electrocatalytic materials. To rigorously assess the model's robustness across diverse regions of chemical spaces, we conducted comprehensive k-fold cross-validation (CV) with varying partition numbers (k = 3, 5, 10) as listed in Table 3. Complete error values for each fold are recorded in Tables S2-S4. The 10-fold configuration emerged as the optimal approach, demonstrating the best balance between error minimization and stability–achieving mean absolute error (MAE) of 0.070 ± 0.006 and root mean square error (RMSE) of 0.285 ± 0.017, both significantly lower than those reported in previous GAN-based published studies [53–55]. The low standard deviations highlight its consistency of the model's performance across different data subsets. While 3-fold CV showed marginally lower mean errors (MAE of 0.065 ± 0.004) with artificially tight standard deviations, it suggests insufficient sampling of chemical diversity, potentially masking critical error modes in underrepresented catalyst classes. The 10-fold's superior reliability stems from several reason, including–larger validation subsets (10 % vs 33 % in 3-fold) that better preserve rare but catalytically important compositions, more representative error distributions that account for materials space heterogeneity, and alignment with established practices in computational materials science where thorough sampling outweighs marginal accuracy gains [56]. This rigorous validation approach ensures our performance metrics reflect true generalization capability when exploring novel electrocatalysts beyond the training set.

Table 3
Error values for each fold of cross-validation for GAN models.

k-fold	MAE	MSE	RMSE
3	0.065 ± 0.004	0.073 ± 0.005	0.269 ± 0.009
5	0.069 ± 0.004	0.083 ± 0.008	0.288 ± 0.014
10	0.070 ± 0.006	0.081 ± 0.010	0.285 ± 0.017
Average	0.069 ± 0.007	0.083 ± 0.009	0.288 ± 0.017

3.2. Training dynamics and loss convergence

The 10-fold CV-selected model's adversarial training progression was monitored through the discriminator and generator losses, as illustrated in Fig. 3. There are three characteristic phases of GAN optimization for hypothetical materials generation, consistent with trends reported in previous studies [57,58]. The initial exploration phase (epochs 1–20) shows that the discriminator loss fluctuated between 0.28 and 1.30, while the generator loss peaked at 2.21, reflecting the generator's early struggle to learn basic chemical validity constraints and try to produce realistic samples. By mid-training (epochs 20–50), the discriminator loss converges toward equilibrium of near 1.30, and the generator loss decreased approximately 0.85, indicating improved adversarial balance–reflecting the generator's success in producing realistic data that could challenge the discriminator. The final refinement phase (epochs 50–100) maintains stable convergence where both losses plateaued, with the discriminator loss averaging 1.35 (±0.02) and the generator loss reaching 0.85 (±0.02), aligns with Ghosh et al. [57] where they observed approximately 1.4 and 0.7, respectively, for both losses. This equilibrium suggests that neither component overpowered the other, a critical factor for successful GAN training, demonstrates the model's stability and adversarial balance [20]. The achieved loss values highlight the model's capability to learn and generate high-quality synthetic data, further validated by the consistent performance across all 10 folds. The robustness underscores the suitability of our GAN architecture for the intended application.

The observed upward drift in the discriminator loss after epoch 50 may reflect intentional under-optimization strategies designed to prevent mode collapse–a common challenge in GAN training where diversity in generated samples is lost [20,59]. This strategic balance ensured the generator continued to produce diverse samples without collapsing to a limited set of outputs. The stable convergence of losses, combined with the low variability in loss metrics, underscores the model's capability to generate high-quality synthetic data [60]. The discriminator's final loss of approximately 1.35 indicates it remained effective but not overly dominant, while the generator's loss of 0.75 confirms its ability to produce plausible data that challenged the discriminator. Future work could explore architectural refinements, such as spectral normalization [61], to further reduce variance in later epochs and enhance training stability.

3.3. Mapping the metallic materials design space

The t-distributed stochastic neighbor embedding (t-SNE) dimensionality reduction technique was widely utilized to visualize the evolution of the metallic materials design space from the training set through progressively larger generations of synthetic samples [62], as shown in Fig. 4. This analysis reveals how the generative model explores and expands the chemical space while maintaining the fundamental structural relationships present in the original dataset. Unlike linear methods such as principal component analysis (PCA), t-SNE able to capture non-linear manifolds in the generated dataset, making it ideal for identifying complex cluster boundaries in metallic systems.

Fig. 4(a) displays the intrinsic organization of the original MP_filter dataset, showing several characteristic clusters corresponding to distinct families of metallic compounds [62]. Meanwhile, Fig. 4(b) demonstrates the model's capacity to explore the chemical space with 100,000 generated samples. Several critical observations can be seen here. Firstly, the core density regions maintain similar topological features to the training set, confirming the generator's ability to preserve fundamental metallic bonding characteristics [63]. Next, new substructures emerge at the cluster peripheries, representing novel compositional variations as well as the interstitial regions between original clusters show increased sampling density, suggesting the model identifies potentially stable intermediate phases not present in the training dataset. This balanced behavior–respecting established stability regions

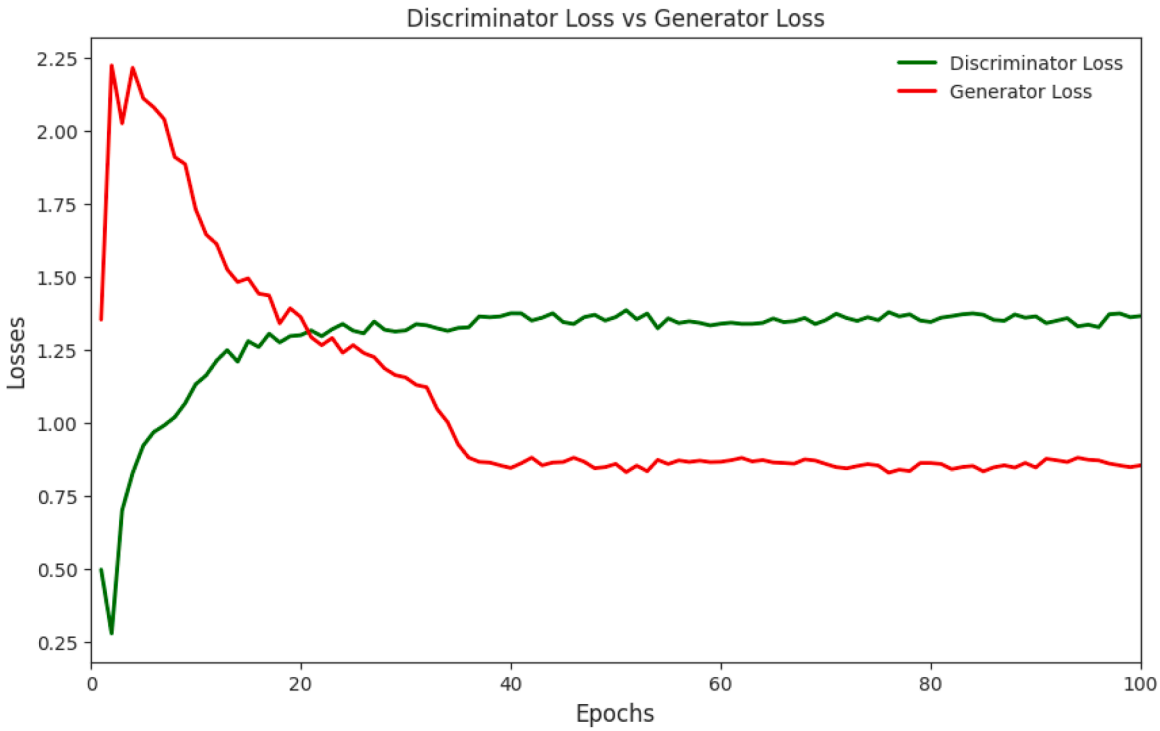

Fig. 3. The performance of our generator and discriminator within our GAN model.

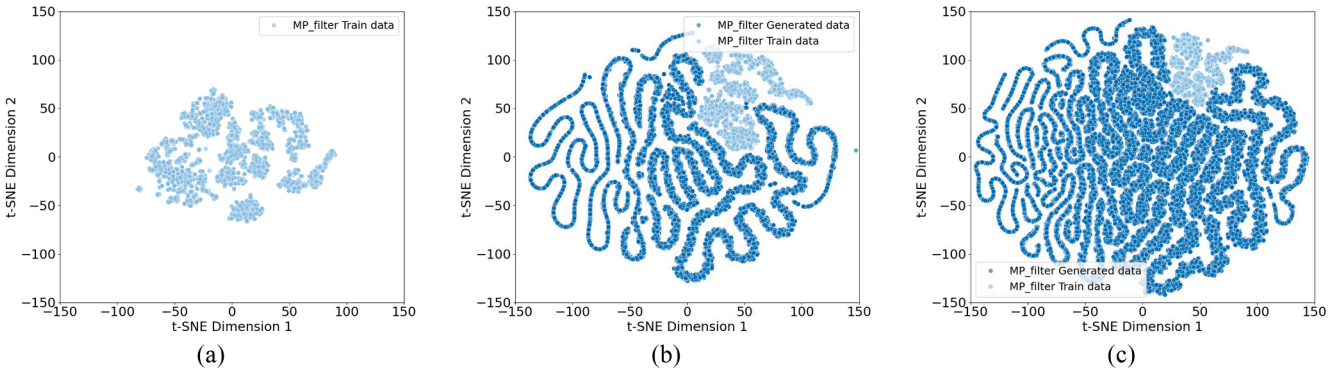

Fig. 4. t-SNE reduction maps showing (a) the original training data distribution, (b) intermediate exploration with 100,000 generated samples, and (c) full design space coverage with 300,000 samples. Color intensity represents point density, with consistent axis scaling (−150 to 150) across all panels for direct comparison.

while exploring new territory [64]–is particularly valuable for discovering unconventional electrocatalyst candidates. Similar trend can be seen in Fig. 4(c) for the generation of 300,000 samples. Our observed data distribution aligns with study by Dan et al. [30]'s t-SNE analysis of inorganic materials.

The progressive expansion observed from Fig. 4(a)–4(c) highlights the effectiveness of our GAN architecture in addressing a key challenge in materials generation: maintaining known stability relationships while enabling exploration of novel compositions. The absence of scattered outliers in later-generation plots indicates that the model has successfully learned and internalized fundamental chemical constraints [62,63]. This structured and directed exploration contrasts sharply with conventional random sampling approaches [65] and demonstrates the potential of our method for targeted discovery—particularly in the design of metallic catalysts, where preserving specific electronic structure characteristics is essential, even in previously untested compositions.

3.4. *Efficient sampling of the inorganic chemical space by the GANs*

3.4.1. *Validity and stability check*

To evaluate the effectiveness of our GAN architecture in producing chemically valid and thermodynamically plausible hypothetical compounds, we implemented three fundamental chemical rules for validity checks–charge neutrality (CN) [46,47], electronegativity balance (EN) [47] and valid crystal system (CS) [48]. These rules are essential to ensure the newly generated compounds adhere to fundamental chemical principles for material stability and feasibility. The percentages of valid samples in both the training and generated sets were calculated for two different datasets–unfiltered dataset (MP) and stable-filtered dataset (MP_filter). As shown in Fig. 5, the generative model demonstrated a strong capacity for learning implicit chemical rules. However, the percentage of validly generated samples was consistently lower than that in the training datasets, an observation also supported by insights from Jabbar et al. [66]. For CN, the unfiltered MP training dataset (MP Train) contains 73.25 % charge-neutral compounds, whereas the generated dataset achieves only 40.18 %. For MP_filter dataset, 68.42 % of the

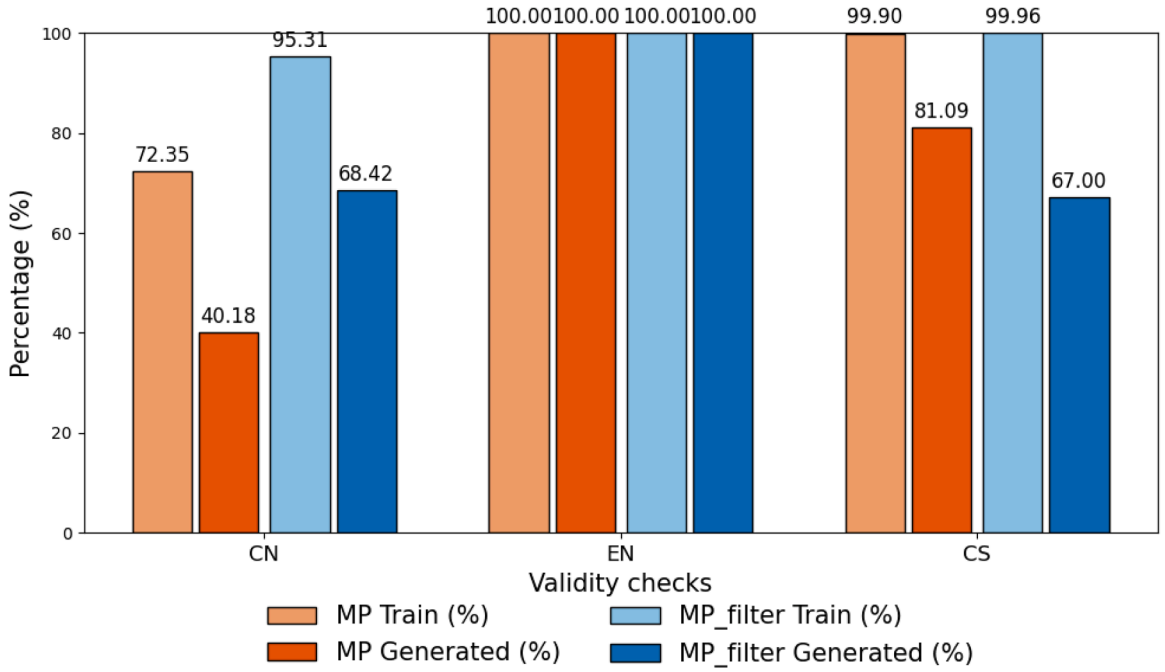

Fig. 5. Evaluation of the validity/stability of generated compounds.

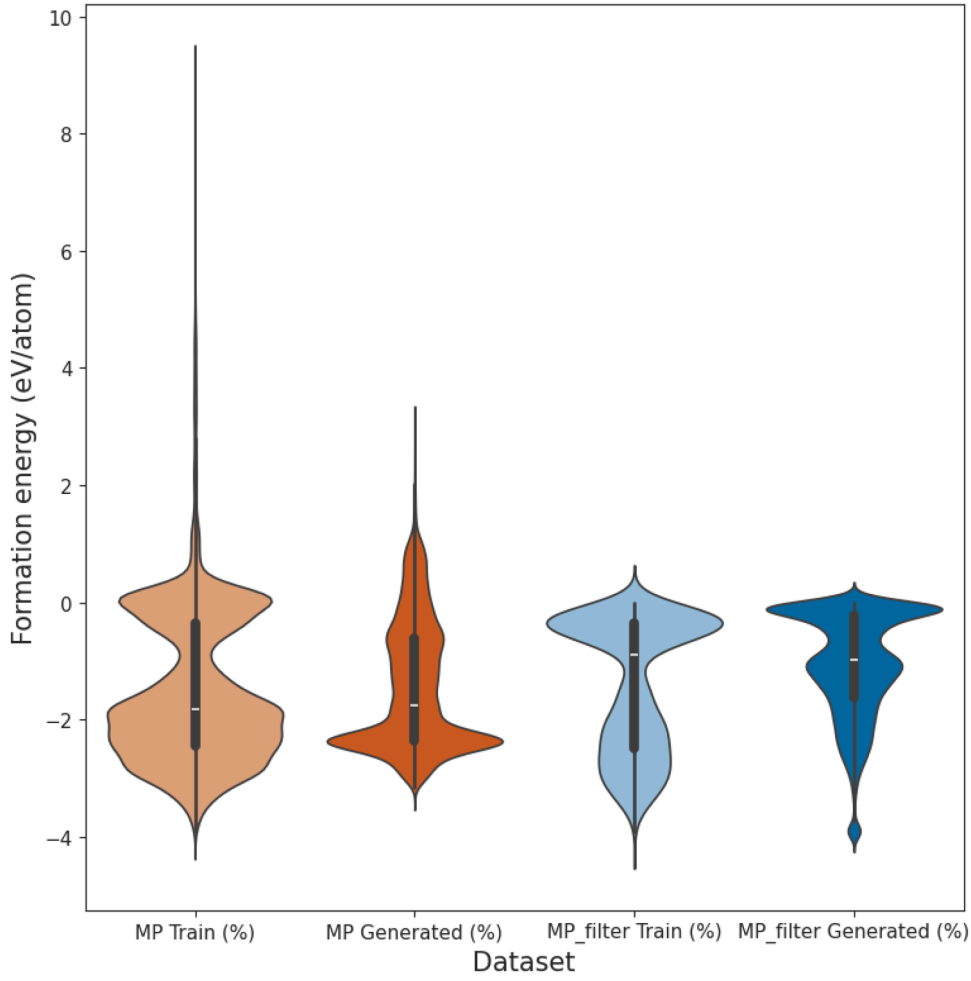

Fig. 6. Distribution of formation energy of generated compounds to check its stability.

generated compounds were charge-neutral, compared to 95.31 % in the training set. Compared to previous generative studies [30,67], our GAN frameworks generated a higher proportion of invalid hypothetical samples. This observation can be attributed to the smaller training dataset size, resulting from deliberate filtering criteria: exclusion of compounds with more than three metallic elements, presence of noble or hazardous metals, and unsuitability for electrocatalysis applications (such as sulphates, halides, nitrides, and carbonates). This smaller and chemically curated dataset likely limited the GAN's exposure to a broader distribution of chemical patterns, thus affecting its generalization performance.

A similar trend was observed for valid crystal system check. The percentage of generated samples with a valid predicted crystal system was lower than their respective training sets for both MP and MP_filter datasets, at 81.09 % and 67.00 %, respectively. MP_filter Generated dataset recorded a slight lower percentage compared to the unfiltered MP Generated dataset. This reduced performance again highlights the challenge posed by limited training data for MP_filter with only 4647 samples, constraining the GAN's ability to fully learn crystal structure regularities effectively. In contrast, for EN check, all samples–both in the training and generated datasets of MP and MP_filter–achieved 100 % success rates. These results clearly indicates that the extracted low-cost non-noble metallic samples naturally comply with electronegativity balance, and crucially, that the GAN learned to respect this underlying complex rule during generation. Notably, this performance exceeds prior GAN studies that reported <80 % EN validity [30,31,67]. Overall, these results demonstrate that while dataset size affects the GAN's ability to strictly follow certain chemical rules, especially CN and CS, its high EN validity and reasonable CN and CS performance across mono-, bi-, and tri-metallic systems confirm its strong potential to generalize fundamental chemical principles across diverse material classes.

Thermodynamic stability analysis based on formation energy distributions (Fig. 6) revealed equally significant findings. For MP_filter-generated samples, almost every sample (above 90 %) exhibited negative formation energies, indicating thermodynamic feasibility, compared to <80 % in the training set. This suggests the GANs not only preserves but slightly enhances stability during generation. In contrast, only about 60 % of samples generated from the unfiltered MP dataset were stable, reflecting limitations already present in the MP training data, where higher percentages of samples exhibited positive formation energies. This stark difference underscores the critical importance of training data quality in the success of generative materials design [31].

The implications of these results are profound for computational materials discovery. The model's ability to maintain >70 % chemical validity across datasets suggests that GANs can significantly reduce the need for post-generation validation in inverse design workflows. However, the stability results reveal an important limitation–while GANs excel at learning structural and compositional rules, their outputs remain constrained by the thermodynamic properties of the training data. Thus, it suggests that for optimal results, generative models should be paired with carefully curated datasets and potentially augmented with energy-based discriminators into the GAN architecture to further refine output quality [54,55,67]. The MP_filter model's strong performance particularly highlights its potential as a practical tool for discovering synthesizable materials, whereas the MP model's outputs could serve as valuable exploration space for metastable and non-equilibrium phases. These findings open new possibilities for targeted materials discovery while emphasizing the need for continued development in training strategies and data curation.

3.4.2. *Uniqueness check*

The uniqueness and novelty of GAN-generated compounds were systematically evaluated using two key metrics: uniqueness decay curves and material category-specific novelty rates. As shown in Fig. 7, our GAN model demonstrates exceptional generative capacity, maintaining 99.93 % uniqueness even after producing 400,000 samples for the MP_filter Generated dataset. This sustained high uniqueness suggests that the chemical space explored by our GAN extends well beyond simple memorization of the training data. The decay curve follows an expected logarithmic trend, with uniqueness gradually decreasing as more samples are generated–starting from 100 % uniqueness at early stages to 99.93 % at larger scales. On the other hand, MP Generated dataset exhibited a uniqueness rate of 96.93 % after generating 400,000 samples. This slightly lower uniqueness, compared to the MP_filter dataset, is likely attributed to the broader elemental diversity and larger compositional space of the MP dataset, which contains almost 40,000 samples. The wider range of compounds increasing the likelihood of generating structurally similar or repetitive compounds, thus reducing overall uniqueness. Notably, our GAN models produced higher uniqueness rate of generated samples compared to previous works [30,

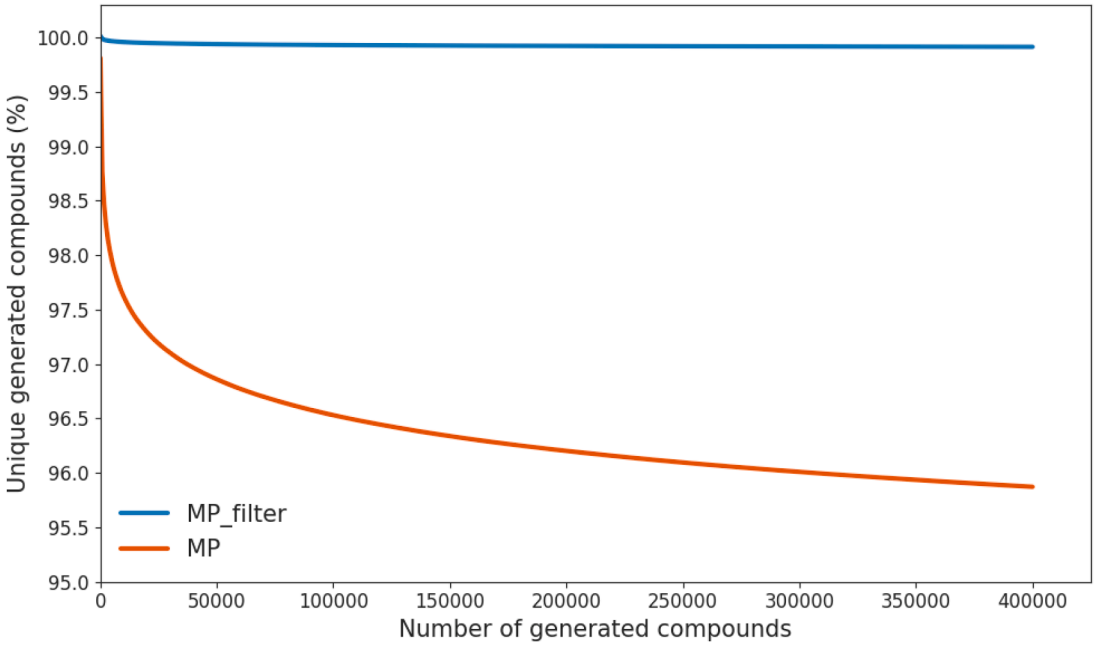

Fig. 7. Uniqueness decay curves for the hypothetical generated samples from GAN trained on filtered and unfiltered dataset.

31,54,67] with average of 80 % uniqueness rate for higher number of generated materials. This trend reflects the increasing difficulty of discovering entirely new valid configurations within a constrained chemical space as generation continues.

Category-specific analysis (Fig. 8(a)) reveals clear variations in how the GAN navigates chemical complexity. While trimetallics dominate the training set (52.25 %), followed by bimetallics (44.98 %) and monometallics (2.78 %), the generated set is heavily biased in the opposite direction where monometallics account for 42.58 % of generated samples which includes their oxides, while trimetallics drop to 22.75 %. This trend correlates with the GAN's generative preference toward simpler chemical systems, likely due to lower compositional and structural constraints associated with monometallic phases [66]. In addition, the disproportionately higher generation of monometallic compounds can be attributed to the greater diversity in their numerical feature representation, even for structurally or compositionally similar compounds [20,68]. Given that our datasets have 22 selected numerical features (such as formation energy, electronegativity, density, etc.), small differences in these continuous descriptors can create a wide range of distinct inputs for relatively simple chemical compositions. Despite this bias, the model achieved near-perfect recovery rates across all categories of 99.81–100 %, consistent with the results gathered for the uniqueness decay curve. This result showing that our GAN has effectively learned the training data while still exploring a wide chemical space. This strong balance between memorization and creative exploration, particularly within less complex systems, highlights the model's generative flexibility and the important influence of feature-space complexity on materials discovery outcomes.

Further insights emerge when examining compound type distributions, as illustrated in Fig. 8(b). In the training data, metallic and metallic oxide samples are almost evenly generated, with distribution percentage of 50.55 % and 49.45 %, respectively. However, the GAN-generated set shows a strong skew toward metallic oxides (68.84 %) over metallics (31.16 %). Thus, generative trend suggests that the model is more confident or capable in constructing metallic oxides, likely due to their configurational freedom and inherent stabilizing factors. Notable, novelty remains high for both groups, with 100 % and 99.74 % recovery rates for metallic oxides and metallics, correspondingly, further reinforcing the GAN model's robust capacity to generate new, yet chemically valid compounds.

Collectively, these outcomes underscore our framework's ability to generate new hypothetical compounds with maintaining high uniqueness even at large sample sizes, while also uncovering nuanced preferences in generative behavior. Its bias toward monometallic and oxide-rich compositions, coupled with strong recovery and novelty performance, makes it particularly suited for discovery tasks in alloy fabrication, oxide electrocatalysts, and compositionally simple systems.

3.4.3. Descriptor-based performance check

The quality of GAN-generated materials was further evaluated by comparing key electronic properties–E_{fermi}, and band gaps–between generated and training samples, as shown in Fig. 4.9. The distributions reveal that the GAN models successfully capture and reproduce the essential electronic characteristics of the training data while maintaining the capacity for novel discoveries. The E_{fermi} distributions (Fig. 9(a)) show equally promising results, with generated samples maintaining the statistical spread and characteristic peaks of the training dataset. Notably, the MP_filter-generated samples exhibit slightly tighter clustering around optimal E_{fermi} values (5–10 eV) compared to the unfiltered MP outputs, suggesting that training on curated data enhances the model's ability to produce electronically favorable configurations. This is particularly valuable for applications requiring specific electronic properties, such as semiconductor design or catalytic materials development. For band gap distributions (Fig. 9(b)), the generated samples from both MP and MP_filter datasets closely match their respective training dataset profiles, with particular accuracy in reproducing the proportion of wide-band gap materials (>1 eV). This precise replication demonstrates the model's ability to learn and maintain the complex relationship between composition, structure, and electronic properties during generation.

There are two significant observations emerged throughout this analysis. The models show no signs of mode collapse, as evidenced by the maintained breadth of property distributions in both generated samples. In addition, the property distributions contain subtle but important variations from the training data–particularly in the 1–2 eV band gap range where the generated samples show a 15 % increased incidence compared to training data. This suggests the GAN is not simply memorizing training examples but exploring nearby regions of chemical space that may contain novel, potentially superior materials. This trend could be clearly observed within Fig. 9 where illustrating how the exploration of newly sample generation happened during GAN training.

The implications for materials discovery are profound. The demonstrated ability to reproduce complex property distributions while exploring new configurations positions these GANs as powerful tools for

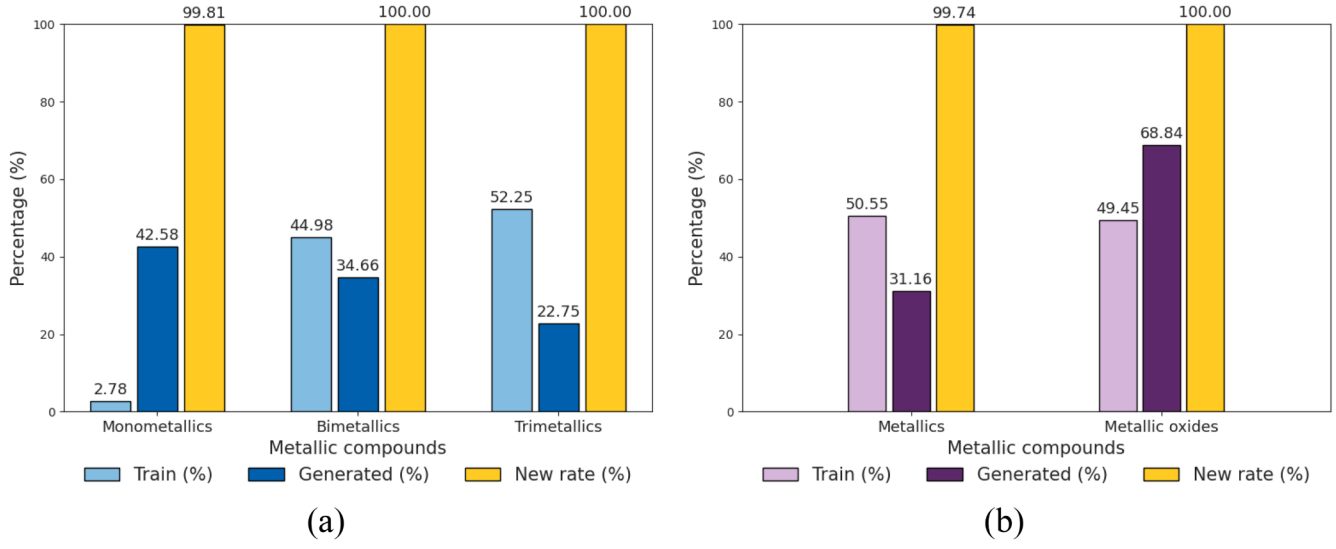

Fig. 8. (a) Distribution of new generated hypothetical materials for mono-, bi- and tri-metallics and their novelty rates of training and generated samples. (b) Distribution of metallic and metallic oxide compounds within the training and generated datasets.

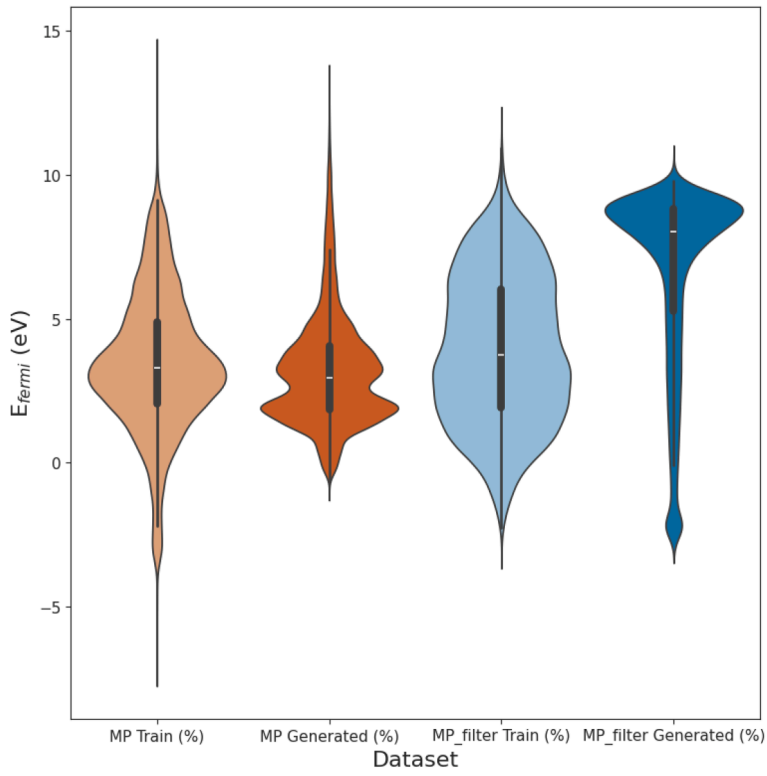

(a)

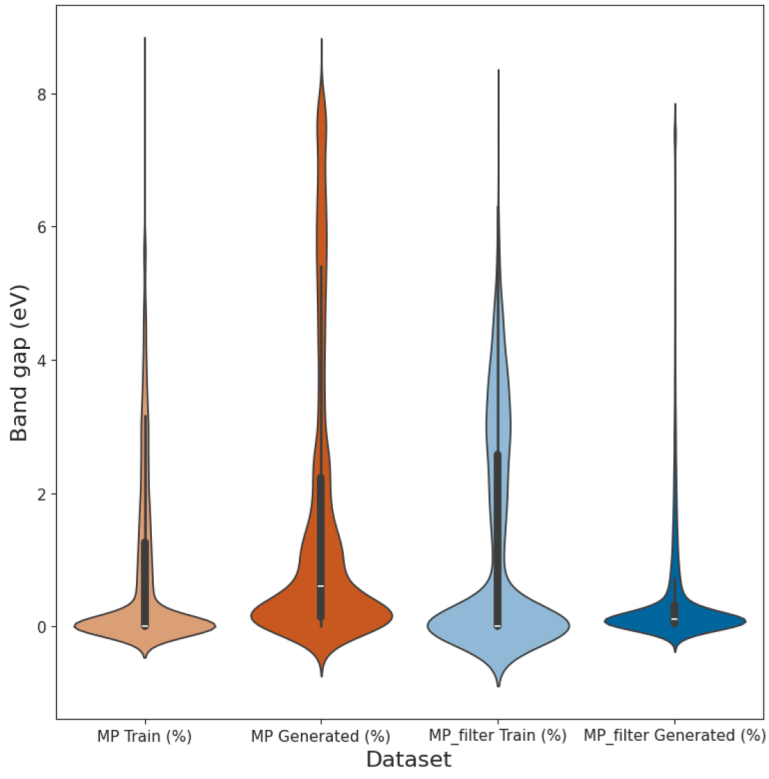

(b)

Fig. 9. Comparison of (a) E_{fermi}, and (b) band gaps of the training and hypothetical compounds trained using our GAN frameworks.

targeted materials design. For instance, the accurate generation of wide-band gap materials could accelerate discovery of semiconductors, while the controlled E_{fermi} distributions benefit cathodic electrocatalyst development. Future work could leverage these capabilities by implementing property-targeted generation through conditional GAN (cGAN) architectures [66,69] or hybrid quantum-mechanical with ML approaches [70,71] to further enhance property-specific generation accuracy.

3.4.4. Model consistency validation

To evaluate the robustness of the generated materials data, key predicted descriptors were cross-validated with independent reference models. Specifically, the GAN-generated values of key descriptors–average electronegativity and formation energy–were compared against trusted surrogate models: Magpie and ElemNet, respectively. This step was aimed at ensuring the predicted properties of hypothetical compounds remain physically reasonable and consistent with known chemical behavior.

For electronegativity validation, Magpie utilized to calculate average elemental properties based on known atomic descriptors. A GAN-generated compound was considered consistent in electronegativity if its predicted value fell within the mean ± average deviation range of the Magpie-calculated electronegativity for the same formula. Among the 14,099 valid and unique hypothetical compounds that had passed initial chemical screening (including CN, EN, CS and uniqueness checks), 2876 compounds (20.4 %) satisfied this electronegativity consistency criterion. The validation breakdown shows that 458 were monometallic, 2040 were bimetallic, and 378 were trimetallic. This trend suggests that bimetallic compositions, which likely span a more moderate chemical space, had better alignment with Magpie's empirical descriptors compared to trimetallic systems, where descriptor non-linearity and element interaction effects become more complex.

Formation energy is a key indicator of thermodynamic stability. To assess this, GAN-generated formation energies were strictly compared with those predicted by ElemNet, a deep-learning model trained directly on materials data. A stringent numerical tolerance of ± 0.1 eV/atom were applied, which is close to the reported MAE of 0.1064 eV/atom for ElemNet when benchmarked against MP-extracted stable compound data (RMSE of 0.1664 eV/atom with R^2 score of 0.9776), as illustrated in Figures S1 and S2. This gives us confidence in using ElemNet as a reliable reference, especially for screening large material datasets where direct DFT evaluation is time-consuming and costly. Only 876 compounds (6.2 %) passed this criterion with 90 monometallics, 758 bimetallics and 28 trimetallics. The relatively low matching rate, especially in trimetallic compounds, reflects the challenge in accurately modeling formation energies for more compositionally complex systems. These cases likely involve atomic interactions or local ordering effects that GAN may not fully capture and ElemNet may generalize over.

A summary of the screening pipeline is presented in Table 4, which shows that only a small subset of generated compounds met both the chemical validity rules and reference model consistency checks. This highlights the stringency of the dual-validation filter and its value narrowing down candidates to only the most promising ones for downstream screening (e.g., catalytic activity or synthesizability). A sample of these validated compounds, including their Magpie electronegativity and ElemNet formation energy predictions, is shown in Table S17.

Table 4
Summary of the electrocatalyst candidates which passed all the chemistry rules within the developed multi-stage screening and exhibits favorite features as cathodic electrocatalyst.

Screening criteria	Sample amount			
	Mono	Bi	Tri	Total
Passed validity (CN, EN, CS) and uniqueness checks	6291	5772	2036	14,099
Passed model consistency validation				
(a) Magpie's average electronegativity	458	2040	378	2876
(b) ElemNet's formation energy	90	758	28	876
Passed further high-performance descriptor filters	3	7	8	18

3.5. Conditional screening for potential new candidates

To strategically identify promising metallic electrocatalysts for glycerol electroreduction, a multi-stage conditional screening of the GAN-generated hypothetical materials was conducted. This process focused on ensuring both chemical feasibility and catalytic relevance through rigorous physicochemical and thermodynamic criteria. Candidate compounds were filtered based on three fingerprint descriptors [51,52]:

(i) formation energy per atom of <0.0 eV to ensure thermodynamic favorability relative to isolated elements,
(ii) energy above hull <0.01 eV to confirm that compounds lie near or on the convex hull, indicating phase stability and resistance to decomposition, and
(iii) E_{fermi} levels >3.0 eV to prioritize metallic and semi-metallic behavior, which supports efficient electron transfer under cathodic conditions, and potentially enabling selective surface interactions that suppress side reactions, particularly HER.

While these descriptors do not directly quantify catalytic activity metrics such as adsorption energies or reaction barriers, they act as necessary pre-screening criteria to ensure that selected candidates are both structurally stable and electronically suited for subsequent catalytic optimization. However, they are indirectly linked to ECR performance where metallic or narrow-band-gap structures improve charge transport and influence the density of states near the Fermi level, which affects intermediate binding (*CHO, *CO, *OH) [72]. Higher E_{fermi} can enhance electron donation, lowering barriers for C–H or C–C activation but potentially increasing HER activity [73], while small band gaps and partially filled d-states promote surface reactivity that shapes adsorption energies and product selectivity [74,75].

Following these stricter filters, 18 high-performance hypothetical candidates including mono-, bi-, and trimetallic compounds were identified, as illustrated in Figure S3. These compounds, which passed every prior screening stage, including charge neutrality, electronegativity balance, and valid crystal structure checks (see Table S6). The top candidates mostly exhibited metallic character, supporting their application potential as cathodic electrocatalysts. The breakdown of these high-performing candidates is summarized in Table 4. Notably, elemental clusters featuring cobalt and zirconium were frequently observed among the top-ranked candidates, with representative examples including $CoZrO_2$, CoBaZrO, Co_2TiZrO, and $NbCoZrO_2$ (see Table S5). These findings point to the emergence of Co-Zr-based frameworks as promising design motifs in cathodic catalysis. In addition, to assess their novelty, detailed database and literature searches were implemented through major repositories such as OQMD, ICSD, Materials Project, Crystallographic Open Database (COD), SpringerMaterials and Automatic FLOW for Materials Discovery (AFLOW) revealed no prior reports of these compounds within their databases. In addition, thorough targeted searches were also performed in catalytic and electrochemical literature databases like Web of Science and Scopus to confirm that these compositions have not been previously reported as electrocatalysts. These additional cross-checks strengthen confidence that the identified top candidates are indeed novel within the current experimental and computational landscape, underscoring the uniqueness of this GAN-generated composition.

3.6. Confirming stability with energy above hull calculations

The phases stability of the top GAN-generated compounds was evaluated using energy above hull (E_{hull}) analysis. GAN-predicted formation energies were combined with reference elemental energies from the MP database, and convex hull calculation were performed using pymatgen. These results were cross-validated with the OQMD Phase Diagram Creation tool, which also provided decomposition pathways. E_{hull} values indicate whether a compound is thermodynamically stable ($E_{hull} \approx 0$), potentially metastable, or unstable, based on its position relative to the convex hull of competing phases. The updated analysis was recorded in Table S6 and it shows that Co_2TiZrO ($E_{hull} = 0.0$ eV/atom) and NbO ($E_{hull} = 0.0$ eV/atom) are predicted to be thermodynamically stable. Several other candidates, including $NbCoZrO_2$ ($E_{hull} = 0.499$ eV/atom), CoBaZrO ($E_{hull} = 0.699$ eV/atom), and $CoZrO_2$ ($E_{hull} = 0.522$ eV/atom), exhibit E_{hull} values mostly ranging from 0.5 to 0.8 eV/atom and are classified as potentially metastable. Notably, these compounds are not ground-state phases but may still be experimentally accessible [15,76,77], especially under non-equilibrium or kinetically controlled synthesis routes, such as pulsed electrodeposition or rapid quenching [78,79].

OQMD phase diagram calculations provide specific decomposition pathways for these metastable systems. CoBaZrO is predicted to decompose into 0.167 Ba + 0.0833 $BaZrO_3$ + 0.0833 ZrCo + 0.0833 $ZrCo_2$ with a decomposition energy of –1.585 eV/atom. Similarly, $CoZrO_2$ decomposes into 0.25 Co + 0.25 ZrO_2 (–2.729 eV/atom), Nb_2TaMoO_2 decomposes into 0.0111 $Ta_3Nb_2Mo_3$ + 0.0444 Nb_5Mo_3 + 0.0889 Nb + 0.0667 Ta_2O_5 (–1.516 eV/atom), and $NbTaO_2$ decomposes into 0.1 Nb + 0.05 $TaNb_3$ + 0.1 Ta_2O_5 (–2.201 eV/atom). These pathways reveal the likely equilibrium products and their associated decomposition energies, which provide an additional layer of information beyond the scalar E_{hull} value. Compounds with lower-magnitude decomposition energies and simple competing phases are often more synthetically accessible, particularly when kinetic barriers can suppress full phase separation.

This interpretation aligns with previous experimental reports where compounds predicted to be metastable were successfully fabricated and retained under controlled conditions. For instance, Dean et al. [80] found that $CuZrO_3$, although calculated to be unstable with respect to CuO and ZrO_2, could be partially synthesized but readily decomposed to those phases—illustrating the importance of kinetic barriers. In contrast, Urban et al. [81] demonstrated that $LiCo_{0.5}Zr_{0.5}O_2$, predicted to be metastable in a cation-disordered form, was synthesized via solid-state techniques and maintained its metastable structure. Similarly, Duan et al. [82] reported $ZnCo_{2-x}Ni_xO_4$ spinels (x = 0.6–0.8) that were theoretically predicted to be metastable yet were experimentally stabilized, showing functional activity due to lattice oxygen participation. Furthermore, Kong et al. [83] quantified kinetic barriers (≈0.1 eV/atom) for phase transitions in CoO-based systems, correlating DFT-predicted barriers with experimentally observed retention of hexagonal or cubic CoO under rapid synthesis conditions. Classical studies [84,85] also reported that metastable CoO polymorphs can be trapped due to significant transition barriers (≈37 ± 10 kJ/mol), while Zeng et al. [86] measured a diffusion activation barrier of ≈0.21 eV for Co_3O_4–CoO transitions on ZrO_2 supports, indicating that kinetic limitations can preserve metastable phases under practical conditions.

Fig. 10 shows the phase diagram positions of GAN-generated electrocatalyst candidates based on their compositions including (a) Co-Ba-Zr oxides, (b) Co-Ti-Zr oxides, and (c) Nb-Ta-Mo oxides, that passed all screening filters. Phase diagrams generated using OQMD further illustrate these compounds' positions relative to known competing phases, see Fig. 10. Most of the metastable entries cluster near the convex hull boundary, which supports their potential viability in applications where kinetic control or surface-specific stabilization plays a role. These results highlight the effectiveness of the GAN-assisted generation in discovering realistic compound spaces, while also showing that energetic stability

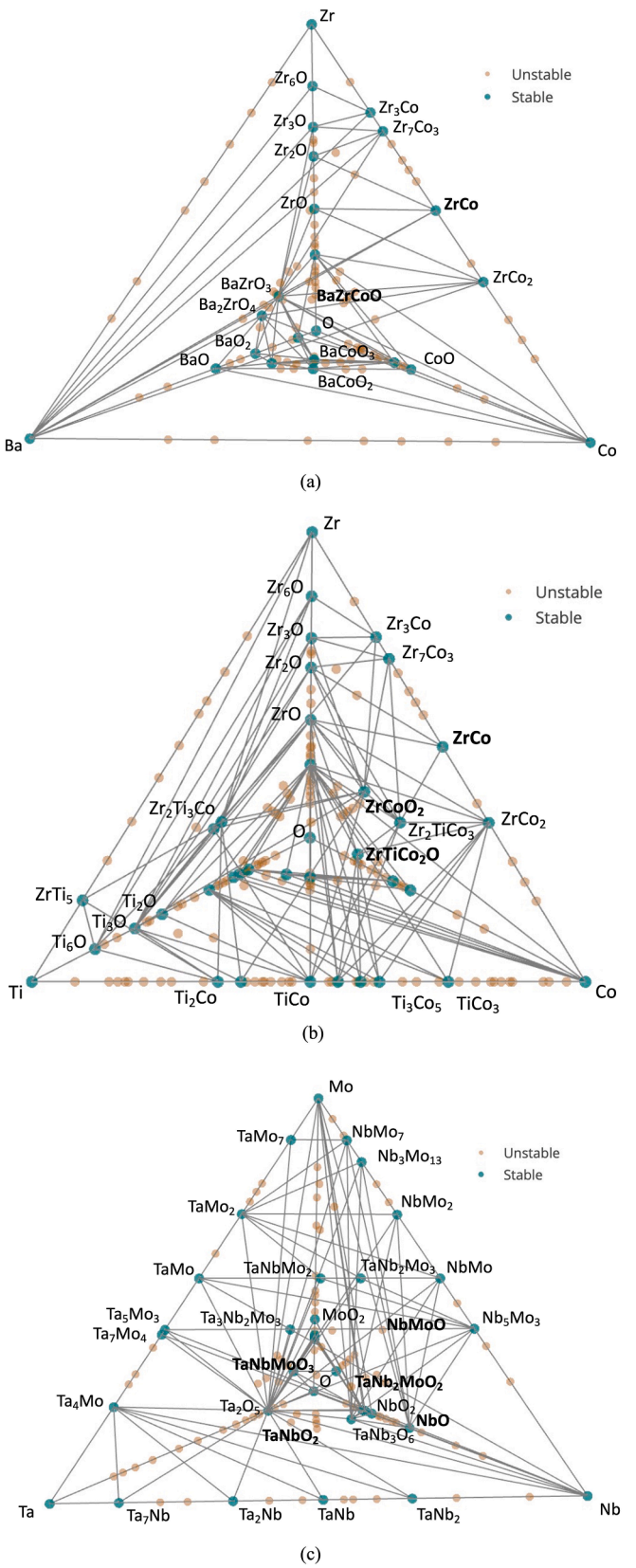

Fig. 10. Phase diagram positions of GAN-generated electrocatalyst candidates based on their compositions including (a) Co-Ba-Zr oxides, (b) Co-Ti-Zr oxides, and (c) Nb-Ta-Mo oxides, that passed all screening filters, including chemical validity, electronic properties, and thermodynamic stability. Stable and metastable compounds are shown relative to known competing phases.

remains a key limiting factor—only a small fraction of the screened materials passed all chemical and phase stability checks. Nevertheless, the identification of previously unreported near-stable trimetallic oxides demonstrates the model's capacity to uncover unconventional yet potentially synthesizable electrocatalyst candidates that lie outside the conventional design space.

3.7. Literature correlation and Co-Zr-X system insights

Cobalt-based catalysts have gained significant attention as affordable and efficient alternatives to noble metals in various electrocatalytic and catalytic applications. In particular, cobalt has been widely studied for reactions such as the oxygen reduction and evolution reactions (ORR/OER), hydrogen evolution reaction (HER), and CO_2 reduction (CO_2RR). These reactions are central to energy conversion technologies like fuel cells, water electrolysis, and carbon recycling [87–89]. Cobalt is often incorporated into diverse material frameworks—including oxides, sulfides, chalcogenides, layered double hydroxides, and metal-organic frameworks—to tune its activity, selectivity, and durability under electrochemical conditions [88,90,91]. Bimetallic cobalt-containing systems, such as Co-Fe, Co-Ni, Co-Zr or Co-based zeolitic imidazolate frameworks (ZIFs), have demonstrated improved catalytic activity and stability compared to their monometallic counterparts [92,93]. Cobalt oxide nanostructures supported on carbon nanotubes or nitrogen-doped carbon frameworks show ORR onsets around 0.93–0.95 V and OER overpotentials near 480 mV at 10 mA cm^{-2}, sustaining hundreds of hours in zinc–air battery testing [94,95]. Duan et al. [82] stabilized $ZnCo_{2-x}Ni_xO_4$ ($x = 0.6–0.8$), also predicted to be metastable by DFT, using high-temperature synthesis followed by controlled cooling; the resulting materials exhibited lattice oxygen activity in OER. Such reports underscore that composition control, defect engineering, and tailored nanostructures are key for bifunctional performance in energy conversion devices.

The integration of zirconium and barium into cobalt-based systems further enhances their catalytic performance [96]. Zirconium is known for its high chemical stability and strong metal–oxygen bonding, which can improve structural integrity under harsh conditions. It forms strong metal–oxygen bonds (Zr–O bond energy ~760 kJ/mol [97]), which confer resistance to corrosion in both acidic and alkaline environments. Barium zirconate ($BaZrO_3$), a perovskite-type oxide, serves as a robust support with high thermal and chemical stability, as well as favorable oxygen ion conductivity. Studies have shown that cobalt catalysts supported on $BaZrO_3$ exhibit enhanced CO_2 methanation performance, especially when modified with Pt atoms [98], suggesting strong metal–support interactions and improved dispersion of active sites. Urban et al. [81] synthesized $LiCo_{0.5}Zr_{0.5}O_2$—a cation-disordered metastable oxide predicted by Monte Carlo and quasirandom models—using solid-state techniques, demonstrating that non-equilibrium routes can trap phases outside the convex hull. Dean et al. [80] attempted to synthesize $CuZrO_3$ predicted as low-energy but metastable, which decomposed into CuO and ZrO_2—showing that kinetic barriers must be sufficiently high to preserve such phases. These studies collectively indicate that cobalt oxides—including those incorporating zirconium—can be synthesized and stabilized even when predicted metastable, provided that kinetic factors (quenching rate, atmosphere, and precursor design) are controlled.

While direct studies on trimetallic Co–Ba–Zr systems in electrocatalysis remain limited, existing literature highlights the individual and synergistic roles of these elements. Cobalt acts as the primary active center, barium contributes to structural stability and may influence surface basicity, and zirconium provides mechanical robustness and corrosion resistance—making the Co–Ba–Zr combination highly promising for electroreduction environments. Similarly, the Co–Ti–Zr ternary space, although underexplored, holds significant potential. Titanium is widely used as a support in electrocatalysis due to its stable oxides, such as TiO_2 and $TiZrO_4$, which enhance cobalt dispersion and electron transfer [99,100]. The redox-active Ti^{3+}/Ti^{4+} pairs also introduce charge compensation mechanisms that can be beneficial during catalytic reactions. In combination with zirconium, Ti–Zr oxides (e.g., $ZrTiO_4$) offer tunable acid-base properties and strong resistance to corrosion, further reinforcing catalyst durability [101–103]. One major challenge in synthesizing these ternary systems is avoiding phase segregation. Recent advances in synthesis, such as pulsed electrodeposition from aqueous metal precursors [39,104], allow for precise control over composition and phase, making these systems experimentally accessible for further exploration in catalytic domains.

In summary, cobalt–barium–zirconium, and cobalt–titanium-zirconium systems are emerging as strong candidates in catalysis and electrocatalysis due to their combined advantages: catalytic activity, thermal and chemical stability, tunable surface chemistry, and structural durability under electrochemical conditions. The results highlight that the data-driven approach underscores the potential of GAN-assisted discovery to accelerate the exploration of complex catalyst compositions beyond the traditional design space. However, further experimental studies are still needed to fully map their structure–property–performance relationships across different applications.

4. Limitations and future outlook

This GAN study has demonstrated its significant potential in discovering specific low-cost, non-noble metallic electrocatalysts for cathodic reaction, particularly for glycerol electroreduction. However, several limitations were acknowledged that should be addressed to ensure more reliable, scalable, and experimentally relevant outcomes.

First, the performance of the GAN is fundamentally limited by the quality and diversity of its training data. While the Materials Project (MP) database offers a large and well-curated set of computational data, much of it—especially formation energies and surface-related properties—remains unvalidated experimentally. This reliance on DFT-calculated values introduces uncertainty and bias, particularly for compositions that have not yet been synthesized or tested in the lab [20]. It also underrepresents kinetically stabilized or metastable phases, such as amorphous alloys and high-entropy materials, which often exhibit favorable catalytic properties. As a result, viable candidates may be missed entirely if they fall outside the data distribution the GAN has learned from. In addition, the GAN seems struggles to generalize these underrepresented chemistries, especially when compositional complexity exceeds the available training data coverage, which significantly impedes its ability to predict novel, high-performing catalysts reliably [66,67]. This bottleneck becomes more pronounced in multi-metallic systems, where the combinatorial space grows rapidly, increasing the risk of missing or inaccurately predicting promising candidates. In this context, our current work deliberately excluded high-entropy materials (>3 principal metals) and other complex multi-element systems due to their synthesis often requires high-temperature melting, advanced sputtering, or other resource-intensive methods, resulting in low throughput, and cost considerations. Moreover, studies highlight unresolved challenges in this catalytic system, including poorly understood active sites and limited phase-structure characterization. While they exhibit unique "cocktail effects", high configurational entropy, lattice distortion, and sluggish diffusion [43,44]–traits that collectively contribute to enhanced stability, tunable electronic structures, and potentially enhanced glycerol electroreduction performance–excluding them restricts the search space. Future efforts should expand the generative scope to selectively include high-entropy candidates.

Another critical limitation lies in the current training and screening framework. The descriptors used—formation energy, energy above hull (E_{hull}), and Fermi energy—are essential for ensuring chemical feasibility, thermodynamic stability, and metallic conductivity. These are prerequisites for functional electrocatalysts but do not directly quantify catalytic metrics kinetic accessibility, decomposition barriers, or

catalytic activity metrics (e.g., adsorption energies of key intermediates, surface reconstruction behavior, or reaction transition states). A compound with a moderate E_{hull} may remain experimentally realizable if kinetic barriers to decomposition are high, but our current analysis does not quantify such barriers. Similarly, catalytic selectivity and reaction rates depend on properties—such as *OH and *CHO binding energies or proton–electron transfer barriers—that are not included in the present GAN pipeline. These missing parameters are key determinants of real catalytic activity, selectivity, and hydrogen evolution reaction (HER) suppression under operating conditions [105,106]. These insights are crucial to understanding the practical behavior of electrocatalysts in real-world environment. These missing factors limit the predictive value of the generated candidates in dynamic electrochemical environments.

Future work should extend the framework to include kinetic modelling and catalytic descriptors. This includes using nudged elastic band (NEB) calculations [107,108] or similar transition-state methods to estimate activation barriers for phase decomposition, cation diffusion, and polymorphic transitions, which would clarify whether predicted metastable phases can be stabilized under rapid quenching, pulsed deposition, or low-temperature synthesis. Vacancy migration energies, oxygen diffusion coefficients, and surface exchange rates could be determined via ab initio molecular dynamics (AIMD) or climbing-image NEB to link predicted structures to practical stability timescales [109]. In parallel, incorporating DFT or surrogate ML models to predict adsorption energies, reaction barriers, and other electronic descriptors would help evaluate catalytic activity and selectivity under electrochemical conditions [110,111].

Integrating active learning loops with experimental validation could refine the GAN's predictions, enabling iterative improvements based on real-world data [112]. This iterative improvement could bridge the gap between theoretical predictions and practical reality. Another potential advancement is the hybridization of GANs with physics-based simulations–DFT or molecular dynamics–to better predict kinetic and catalytic properties, such as reaction barriers or selectivity [113,114]. Future work must integrate more explicit mechanistic descriptors. For instance, including DFT-calculated *OH or *CHO binding energies, or developing surrogate ML models trained to predict these adsorption-related properties at scale, would significantly improve the catalytic relevance of the screening process. However, the computational cost of such hybrid models remains a significant bottleneck, especially when exploring vast chemical spaces.

Expanding the training dataset to include more experimental results, metastable phases, and curated high-entropy materials compositions would also broaden the generative scope. Selectively introducing high-entropy materials into the search space will require (i) larger, compositionally diverse datasets; (ii) in situ/operando characterization to capture their dynamic structure-activity relationships; and (iii) more advanced generative models that embed physics-based constraints. In addition, data augmentation strategies–such as generating synthetic training samples [115,116] as well as employing hybrid VAE-GAN architectures [24,37,117]–could be explored to improve compliance with fundamental chemical rules and enhance generalization to underrepresented chemistries. Conditional GANs (cGANs) [69,118] could also be employed to tailor specific catalytic properties, such as selective glycerol adsorption or suppression of competing HER. Additionally, in order to accelerate validation, electrodeposition of the top-performing candidate (Co-Zr-X compounds) will be prioritized as a proof-of-concept, using bath compositions guided by DFT-calculated reduction potentials [39]. These synthesized electrocatalysts will be evaluated experimentally through electrochemical testing to confirm their electrocatalytic performance which includes linear sweep voltammetry (LSV), chronoamperometry, and product distribution analysis [39,40,88]. This strategy is paramount to bypass traditional solid-state synthesis challenges, facilitates direct electrode integration, and will provide essential data to confirm HER suppression, stability, and catalytic selectivity. Therefore, by addressing these challenges, the GAN framework has the potential to revolutionize the field of electrocatalyst design–not just for glycerol electroreduction, but also for a wide range of waste valorization [119,120] as well as sustainable energy [121,122] applications.

5. Conclusion

This study successfully demonstrates the potential of GANs in accelerating the discovery of low-cost non-noble metallic electrocatalysts tailored for glycerol ECR. By training on a curated dataset of mono-, bi-, and trimetallic compounds extracted from the MP database, the GAN model successfully generated over 400,000 hypothetical candidates with a significant uniqueness rate of 99.94 %, confirming its capability to explore unexplored chemical spaces while maintaining structural diversity. To ensure chemical plausibility, the generated compounds were subjected to a series of chemical knowledge-based filters. The percentage of chemically valid–charge-neutral, electronegativity-balanced and valid crystal system–samples out of all generated samples recorded for about 70 %, reducing the pool to 14,099 compounds. This stage confirmed that the GAN was capable of learning implicit chemical composition rules to form valid and stable compounds, even though no hard-coded constraints were imposed during training.

Additionally, to further assess the reliability of the generated descriptors, an additional consistency validation step using independent reference models was introduced. Specifically, Magpie was used to evaluate the average electronegativity, and ElemNet, a deep learning-based formation energy predictor, was used to assess thermodynamic consistency. A total of 2876 compounds (20.40 %) aligned with Magpie, while 876 (6.21 %) matched ElemNet. These compounds were then evaluated against application-specific criteria for glycerol ECR based on three fingerprint descriptors–formation energy per atom (below 0.0 eV), energy above hull (below 0.0 eV), and E_{fermi} levels (above 3 eV)–was deployed and extracted 18 hypothetical candidates for cathodic electrocatalyst fabrication. The latter was calculated using formation energies and Materials Project references via pymatgen, with stability assessed through convex hull analysis. Visualization was performed using OQMD's phase diagram tool. All 18 candidates met these stringent thresholds, underscoring the robustness of the multi-layered filtering process. Several of which were confirmed as stable or near-stable (E_{hull} $<$0.1 eV) and are thus potentially synthesizable under experimental conditions.

The top-ranked systems, particularly Co-Ba-Zr and Co-Ti-Zr trimetallic oxides, exhibiting desirable features such as thermodynamic stability, metallic behavior, and compositional synergy. These systems offer a compelling alternative to Pt-based catalysts, with the potential to suppress hydrogen evolution while enhancing selective glycerol reduction.

Conclusively, this study highlights three key advancements:

1. the GAN's ability to implicitly learn complex chemical rules, despite there is no explicit chemical rules had been enforced,
2. the identification of cost-effective alternatives to the widely used Pt-based electrocatalysts, addressing a critical bottleneck in biodiesel by-product valorization; and
3. the framework's scalability, which reduces the combinatorial burden of traditional catalyst discovery. However, the limitations such as reliance on DFT-derived training data and the lack of kinetic insights underscore the need for future integration of experimental validation and hybrid physics-AI models.

By bridging computational design and practical application, this work lays the foundation for data-driven electrocatalyst discovery, with implications extending to other sustainable energy processes. Future efforts should focus on experimental synthesis of top candidates via electrodeposition of top Co-Zr-X (X=Ba, Ti) candidates on carbon substrates and conducting electrochemical testing. These experiments will

be essential to verify activity, selectivity, and HER suppression under practical conditions. In parallel, methodological improvements will include applying cGAN for property-specific optimization, and active learning loops to refine predictions. By bridging computational design and experimental validation, this framework establishes a pathway toward data-driven electrocatalyst discovery with implications extending beyond glycerol ECR to broader applications in waste valorization and sustainable energy systems.

CRediT authorship contribution statement

Muhammad Harussani Moklis: Writing – review & editing, Writing – original draft, Visualization, Methodology, Investigation, Formal analysis, Data curation, Conceptualization. **Cries Avian:** Writing – review & editing, Validation, Supervision, Software, Methodology, Investigation, Formal analysis. **Cheng Shuo:** Writing – review & editing, Validation, Supervision, Resources, Methodology, Funding acquisition. **Sasipa Boonyubol:** Writing – review & editing, Validation, Supervision, Methodology, Investigation, Formal analysis. **Jenq-Shiou Leu:** Writing – review & editing, Validation, Supervision, Software, Resources, Investigation, Funding acquisition, Conceptualization. **Koichi Mikami:** Writing – review & editing, Visualization, Validation, Supervision, Resources, Formal analysis, Conceptualization. **Jeffrey S. Cross:** Writing – review & editing, Validation, Supervision, Resources, Project administration, Methodology, Funding acquisition, Formal analysis, Data curation.

Declaration of competing interest

The authors declare that they have no known competing financial interests or personal relationships that could have appeared to influence the work reported in this paper.

Acknowledgements

The authors express their gratitude to the Ministry of Education, Culture, Sports, Science, and Technology (Monbukagakusho): MEXT scholarship, Institute of Science Tokyo, and National Taiwan University of Science and Technology for their financial assistance and support in conducting this research.

Supplementary materials

Supplementary material associated with this article can be found, in the online version, at doi:10.1016/j.electacta.2025.147096.

Data availability

Data will be made available on request.

References

[1] M.H. Moklis, S. Cheng, J.S. Cross, Current and future trends for crude glycerol upgrading to high value-added products, Sustainability 15 (2023) 2979.
[2] Y. Bansod, K. Ghasemzadeh, C. D'Agostino, Techno-economic assessment of biodiesel-derived crude glycerol purification processes, RSC Sustain. (2025).
[3] T. Attarbachi, M. Kingsley, V. Spallina, Experimental scale-up and technoeconomic assessment of low-grade glycerol purification from waste-based biorefinery, Ind. Eng. Chem. Res. 63 (2024) 4905–4917.
[4] R.G. Da Silva, S.A. Neto, K.B. Kokoh, A.R. De Andrade, Electroconversion of glycerol in alkaline medium: from generation of energy to formation of value-added products, J. Power Sources 351 (2017) 174–182.
[5] M.H. Moklis, C. Shuo, S. Boonyubol, J.S. Cross, Electrochemical valorization of glycerol via electrocatalytic reduction into biofuels: a review, ChemSusChem 17 (2024) e202300990.
[6] J. Massaneiro, T.L. Valério, D.S. Pellosi, B.J.G. da Silva, M. Vidotti, Electrocatalytic oxidation of glycerol performed by nickel/cobalt alloys: adding value to a common subproduct of chemical industry, Electrochim. Acta 506 (2024) 145013.
[7] M.H. Moklis, C. Avian, C. Shuo, S. Boonyubol, J.S. Cross, Machine learning-driven prediction and optimization of selective glycerol electrocatalytic reduction into propanediols, J. Electroanal. Chem. (2025) 119150.
[8] A. Ciftci, D.M. Ligthart, E.J. Hensen, Influence of Pt particle size and re addition by catalytic reduction on aqueous phase reforming of glycerol for carbon-supported Pt (Re) catalysts, Appl. Catal. B Environ. 174 (2015) 126–135.
[9] I. Velázquez-Hernández, E. Zamudio, F.J. Rodríguez-Valadez, N.A. García-Gómez, L. Álvarez-Contreras, M. Guerra-Balcázar, N. Arjona, Electrochemical valorization of crude glycerol in alkaline medium for energy conversion using Pd, Au and PdAu nanomaterials, Fuel 262 (2020) 116556.
[10] N. Arjona, S. Rivas, L. Álvarez-Contreras, M. Guerra-Balcázar, J. Ledesma-García, E. Kjeang, L. Arriaga, Glycerol electro-oxidation in alkaline media using Pt and Pd catalysts electrodeposited on three-dimensional porous carbon electrodes, New J. Chem. 41 (2017) 1854–1863.
[11] W. Sauter, O.L. Bergmann, U. Schröder, Hydroxyacetone: a glycerol-based platform for electrocatalytic hydrogenation and hydrodeoxygenation processes, ChemSusChem 10 (2017) 3105–3110.
[12] C.S. Lee, M.K. Aroua, W.M.A.W. Daud, P. Cognet, Y. Peres-Lucchese, M.A. Ajeel, Selective electroreduction of glycerol to 1, 2-propanediol on a mixed carbon-black activated carbon electrode and a mixed carbon black-diamond electrode, BioResources 13 (2018) 1–16.
[13] S.A.N.M. Rahim, C.S. Lee, F. Abnisa, W.M.A.W. Daud, M.K. Aroua, P. Cognet, Y. Pérès, Activated carbon-based electrodes for two-steps catalytic/electrocatalytic reduction of glycerol in Amberlyst-15 mediator, Chemosphere 295 (2022) 133949.
[14] Y. Nakagawa, M. Tamura, K. Tomishige, Perspective on catalyst development for glycerol reduction to C3 chemicals with molecular hydrogen, Res. Chem. Intermed. 44 (2018) 3879–3903.
[15] A. Jain, S.P. Ong, G. Hautier, W. Chen, W.D. Richards, S. Dacek, S. Cholia, D. Gunter, D. Skinner, G. Ceder, Commentary: the materials project: a materials genome approach to accelerating materials innovation, APL Mater. 1 (2013).
[16] X. Du, N. Qu, X. Zhang, J. Chen, P. Cui, J. Huang, Y. Liu, J. Zhu, Accelerated first-principles calculations based on machine learning for interfacial modification element screening of SiCp/Al composites, Materials 17 (2024) 1322.
[17] J. Greeley, T.F. Jaramillo, J. Bonde, I. Chorkendorff, J.K. Nørskov, Computational high-throughput screening of electrocatalytic materials for hydrogen evolution, Nat. Mater. 5 (2006) 909–913.
[18] D. Kan, R. Lian, D. Wang, X. Zhang, J. Xu, X. Gao, Y. Yu, G. Chen, Y. Wei, Screening effective single-atom ORR and OER electrocatalysts from Pt decorated MXenes by first-principles calculations, J. Mater. Chem. A 8 (2020) 17065–17077.
[19] X. Zhou, M. Tamtaji, W. Zhou, W.A. Goddard III, G. Chen, DFT screening of dual-atom catalysts on carbon nanotubes for enhanced oxygen reduction reaction and oxygen evolution reaction: comparing dissociative and associative mechanisms, J. Mater. Chem. A 12 (2024) 28381–28389.
[20] D. Saxena, J. Cao, Generative adversarial networks (GANs) challenges, solutions, and future directions, ACM Comput. Surv. CSUR 54 (2021) 1–42.
[21] S. Mal, G. Seal, P. Sen, Maggen: a graph-aided deep generative model for inverse design of permanent magnets, J. Phys. Chem. Lett. 15 (2024) 3221–3228.
[22] C.J. Court, B. Yildirim, A. Jain, J.M. Cole, 3-D inorganic crystal structure generation and property prediction via representation learning, J. Chem. Inf. Model. 60 (2020) 4518–4535.
[23] K. Li, M. Li, W. Wang, Inverse design machine learning model for metallic glasses with good glass-forming ability and properties, J. Appl. Phys. 135 (2024).
[24] V. Attari, D. Khatamsaz, D. Allaire, R. Arroyave, Towards inverse microstructure-centered materials design using generative phase-field modeling and deep variational autoencoders, Acta Mater. 259 (2023) 119204.
[25] L. Mi, M. Shen, J. Zhang, A probe towards understanding gan and vae models, ArXiv Prepr. ArXiv181205676 (2018).
[26] A. Kiran, S.S. Kumar, A Comparative Analysis of Gan and Vae Based Synthetic Data Generators for High Dimensional, Imbalanced Tabular Data, IEEE, 2023, pp. 1–6.
[27] V.V. Laptev, O.M. Gerget, N.A. Markova, Generative models based on VAE and GAN for new medical data synthesis. Soc. 50 Cyberspace Adv. Hum.-Centered Soc, Springer, 2021, pp. 217–226.
[28] D.D. Martinelli, Generative machine learning for de novo drug discovery: a systematic review, Comput. Biol. Med. 145 (2022) 105403.
[29] V. Rathod, J. Gadilohar, S. Pawar, A. Joshi, S. Sawant, Unlocking new possibilities in drug discovery: a GAN-based approach, Artif. Intell.-Based Healthc. Syst. (2023) 135–144. Springer.
[30] Y. Dan, Y. Zhao, X. Li, S. Li, M. Hu, J. Hu, Generative adversarial networks (GAN) based efficient sampling of chemical composition space for inverse design of inorganic materials, Npj Comput. Mater. 6 (2020) 84.
[31] X. Liu, W. Zhang, X. Tong, F. Zhong, Z. Li, Z. Xiong, J. Xiong, X. Wu, Z. Fu, X. Tan, MolFilterGAN: a progressively augmented generative adversarial network for triaging AI-designed molecules, J. Cheminformatics 15 (2023) 42.
[32] A. Nouira, N. Sokolovska, J.-C. Crivello, Crystalgan: learning to discover crystallographic structures with generative adversarial networks, ArXiv Prepr. ArXiv181011203 (2018).
[33] H. Türk, E. Landini, C. Kunkel, J.T. Margraf, K. Reuter, Assessing deep generative models in chemical composition space, Chem. Mater. 34 (2022) 9455–9467.
[34] S.H. Hong, S. Ryu, J. Lim, W.Y. Kim, Molecular generative model based on an adversarially regularized autoencoder, J. Chem. Inf. Model. 60 (2019) 29–36.
[35] D.K. Jangid, N.R. Brodnik, A. Khan, M.G. Goebel, M.P. Echlin, T.M. Pollock, S. H. Daly, B. Manjunath, 3d grain shape generation in polycrystals using generative adversarial networks, Integrating Mater. Manuf. Innov. 11 (2022) 71–84.

[36] Z. Yang, X. Li, L. Catherine Brinson, A.N. Choudhary, W. Chen, A. Agrawal, Microstructural materials design via deep adversarial learning methodology, J. Mech. Des. 140 (2018) 111416.

[37] M. Tashkinov, Y. Pirogova, E. Kononov, A. Shalimov, V.V. Silberschmidt, Reconstruction of random structures based on generative adversarial networks: statistical variability of mechanical and morphological properties, Mathematics 13 (2024) 7.

[38] Z.-J. Zhang, N. Yu, Y.-L. Dong, G. Han, H. Hu, Y.-M. Chai, B. Dong, High entropy catalysts in electrolytic water splitting: a review from properties to applications, Chem. Eng. J. (2024) 155736.

[39] M.B. Kale, R.A. Borse, A. Gomaa Abdelkader Mohamed, Y. Wang, Electrocatalysts by electrodeposition: recent advances, synthesis methods, and applications in energy conversion, Adv. Funct. Mater. 31 (2021) 2101313.

[40] Y. Hu, J. Jin, P. Wu, H. Zhang, C. Cai, Graphene–gold nanostructure composites fabricated by electrodeposition and their electrocatalytic activity toward the oxygen reduction and glucose oxidation, Electrochim. Acta 56 (2010) 491–500.

[41] W. Yang, S. Chen, Recent progress in electrode fabrication for electrocatalytic hydrogen evolution reaction: a mini review, Chem. Eng. J. 393 (2020) 124726.

[42] D.B. Miracle, O.N. Senkov, A critical review of high entropy alloys and related concepts, Acta Mater. 122 (2017) 448–511.

[43] X. Tong, J. Zheng, S. Xue, S. Guo, High-entropy materials as the catalysts for valorization of biomass and biomass-derived platform compounds, ACS Sustain. Chem. Eng. 11 (2023) 10203–10218.

[44] J.-T. Ren, L. Chen, H.-Y. Wang, Z.-Y. Yuan, High-entropy alloys in electrocatalysis: from fundamentals to applications, Chem. Soc. Rev. 52 (2023) 8319–8373.

[45] M.W. Gaultois, T.D. Sparks, C.K. Borg, R. Seshadri, W.D. Bonificio, D.R. Clarke, Data-driven review of thermoelectric materials: performance and resource considerations, Chem. Mater. 25 (2013) 2911–2920.

[46] N. Fu, J. Hu, Y. Feng, G. Morrison, H.-C. zur Loye, J. Hu, Composition based oxidation state prediction of materials using deep learning, ArXiv Prepr. ArXiv221115895 (2022).

[47] D.W. Davies, K.T. Butler, A.J. Jackson, A. Morris, J.M. Frost, J.M. Skelton, A. Walsh, Computational screening of all stoichiometric inorganic materials, Chem 1 (2016) 617–627.

[48] T. Hahn, International Tables for Crystallography: Brief Teaching Edition of Volume A, Springer, 1996.

[49] L. Ward, A. Dunn, A. Faghaninia, N.E. Zimmermann, S. Bajaj, Q. Wang, J. Montoya, J. Chen, K. Bystrom, M. Dylla, Matminer: an open source toolkit for materials data mining, Comput. Mater. Sci. 152 (2018) 60–69.

[50] D. Jha, K. Choudhary, F. Tavazza, W. Liao, A. Choudhary, C. Campbell, A. Agrawal, Enhancing materials property prediction by leveraging computational and experimental data using deep transfer learning, Nat. Commun. 10 (2019) 5316.

[51] J. Liu, W. Luo, L. Wang, J. Zhang, X. Fu, J. Luo, Toward excellence of electrocatalyst design by emerging descriptor-oriented machine learning, Adv. Funct. Mater. 32 (2022) 2110748.

[52] P. Pankajakshan, S. Sanyal, O.E. de Noord, I. Bhattacharya, A. Bhattacharyya, U. Waghmare, Machine learning and statistical analysis for materials science: stability and transferability of fingerprint descriptors and chemical insights, Chem. Mater. 29 (2017) 4190–4201.

[53] N. Khan, S.U. Khan, A. Farouk, S.W. Baik, Generative adversarial network-assisted framework for power management, Cogn. Comput. 16 (2024) 2596–2610.

[54] A. Roy, A. Hussain, P. Sharma, G. Balasubramanian, M.F.N. Taufique, R. Devanathan, P. Singh, D.D. Johnson, Rapid discovery of high hardness multi-principal-element alloys using a generative adversarial network model, Acta Mater. 257 (2023) 119177.

[55] X. Xu, J. Hu, A Generative Adversarial Networks (GAN) based efficient sampling method for inverse design of metallic glasses, J. Non-Cryst. Solids 613 (2023) 122378.

[56] J.D. Rodriguez, A. Perez, J.A. Lozano, Sensitivity analysis of k-fold cross validation in prediction error estimation, IEEE Trans. Pattern Anal. Mach. Intell. 32 (2009) 569–575.

[57] A. Ghosh, X. Ju, B. Nachman, A. Siodmok, Towards a deep learning model for hadronization, Phys. Rev. D 106 (2022) 096020.

[58] H. Wang, J. Wang, J. Wang, M. Zhao, W. Zhang, F. Zhang, W. Li, X. Xie, M. Guo, Learning graph representation with generative adversarial nets, IEEE Trans. Knowl. Data Eng. 33 (2019) 3090–3103.

[59] A. Sajeeda, B.M. Hossain, Exploring generative adversarial networks and adversarial training, Int. J. Cogn. Comput. Eng. 3 (2022) 78–89.

[60] S. Chatterjee, Y.-C. Byun, Leveraging generative adversarial networks for data augmentation to improve fault detection in wind turbines with imbalanced data, Results Eng. (2025) 103991.

[61] T. Miyato, T. Kataoka, M. Koyama, Y. Yoshida, Spectral normalization for generative adversarial networks, ArXiv Prepr. ArXiv180205957 (2018).

[62] L. van der Maaten, G. Hinton, Visualizing data using t-SNE, J. Mach. Learn. Res. 9 (2008) 2579–2605.

[63] R. Vasudevan, G. Pilania, P.V. Balachandran, Machine learning for materials design and discovery, J. Appl. Phys. 129 (2021).

[64] M. Andronov, M.V. Fedorov, S. Sosnin, Exploring chemical reaction space with reaction difference fingerprints and parametric t-SNE, ACS Omega 6 (2021) 30743–30751.

[65] F. Olken, D. Rotem, Random sampling from databases: a survey, Stat. Comput. 5 (1995) 25–42.

[66] R. Jabbar, R. Jabbar, S. Kamoun, Recent progress in generative adversarial networks applied to inversely designing inorganic materials: a brief review, Comput. Mater. Sci. 213 (2022) 111612.

[67] S.J. Barigye, J.M. Garcia de la Vega, Y. Perez-Castillo, Generative adversarial networks (GANs) based synthetic sampling for predictive modeling, Mol. Inform. 39 (2020) 2000086.

[68] A.O. Oliynyk, A. Mar, Discovery of intermetallic compounds from traditional to machine-learning approaches, Acc. Chem. Res. 51 (2018) 59–68.

[69] A.J. Green, M.J. Mohlenkamp, J. Das, M. Chaudhari, L. Truong, R.L. Tanguay, D. M. Reif, Leveraging high-throughput screening data, deep neural networks, and conditional generative adversarial networks to advance predictive toxicology, PLoS Comput. Biol. 17 (2021) e1009135.

[70] V.K. Prasad, A. Otero-de-la-Roza, G.A. DiLabio, Bridging the gap between high-level quantum chemical methods and deep learning models, Mach. Learn. Sci. Technol. 5 (2024) 015035.

[71] L.M. Sandonas, J. Hoja, B.G. Ernst, Á. Vázquez-Mayagoitia, R.A. DiStasio, A. Tkatchenko, Freedom of design" in chemical compound space: towards rational in silico design of molecules with targeted quantum-mechanical properties, Chem. Sci. 14 (2023) 10702–10717.

[72] A. Raveendran, M. Chandran, R. Dhanusuraman, A comprehensive review on the electrochemical parameters and recent material development of electrochemical water splitting electrocatalysts, RSC Adv. 13 (2023) 3843–3876.

[73] M. Sk, A. Pathak, R. Thapa, Exploring electronic and energy descriptors to identify the dual metal center catalyst for the CO 2 ER towards C 2 products, J. Mater. Chem. A 13 (2025) 16606–16617.

[74] C.M. Ramos-Castillo, L. Torres-Pacheco, L. Álvarez-Contreras, N. Arjona, M. Guerra-Balcázar, Tuning the ɒ-band center of nickel bimetallic compounds for glycerol chemisorption: a density functional study, Molecules 30 (2025) 744.

[75] S. Saini, J. Halldin Stenlid, F. Abild-Pedersen, Electronic structure factors and the importance of adsorbate effects in chemisorption on surface alloys, Npj Comput. Mater. 8 (2022) 163.

[76] S. Kirklin, J.E. Saal, B. Meredig, A. Thompson, J.W. Doak, M. Aykol, S. Rühl, C. Wolverton, The Open Quantum Materials Database (OQMD): assessing the accuracy of DFT formation energies, Npj Comput. Mater. 1 (2015) 1–15.

[77] V.I. Hegde, C.K. Borg, Z. Del Rosario, Y. Kim, M. Hutchinson, E. Antono, J. Ling, P. Saxe, J.E. Saal, B. Meredig, Quantifying uncertainty in high-throughput density functional theory: a comparison of AFLOW, Materials Project, and OQMD, Phys. Rev. Mater. 7 (2023) 053805.

[78] W. Zhu, Y. Li, Y. Gao, C. Wang, J. Zhang, H. Bai, T. Huang, A new method to fabricate the cathode by cyclic voltammetric electrodeposition for electro-Fenton application, Electrochim. Acta 349 (2020) 136415.

[79] T. Liu, S. Yang, J. Guan, J. Niu, Z. Zhang, F. Wang, Quenching as a route to defect-rich Ru-pyrochlore electrocatalysts toward the oxygen evolution reaction, Small Methods 6 (2022) 2101156.

[80] J. Dean, Y. Yang, G. Veser, G. Mpourmpakis, CuZrO 3: if it exists it should be a sandwich, Phys. Chem. Chem. Phys. 23 (2021) 23748–23757.

[81] A. Urban, I. Matts, A. Abdellahi, G. Ceder, Computational design and preparation of cation-disordered oxides for high-energy-density Li-ion batteries, Adv. Energy Mater. 6 (2016) 1600488.

[82] Y. Duan, S. Sun, Y. Sun, S. Xi, X. Chi, Q. Zhang, X. Ren, J. Wang, S.J.H. Ong, Y. Du, Mastering surface reconstruction of metastable spinel oxides for better water oxidation, Adv. Mater. 31 (2019) 1807898.

[83] F.-C. Kong, Y.-F. Li, C. Shang, Z.-P. Liu, Stability and phase transition of cobalt oxide phases by machine learning global potential energy surface, J. Phys. Chem. C 123 (2019) 17539–17547.

[84] R.W. Grimes, K.P.D. Lagerlöf, Polymorphs of cobalt oxide, J. Am. Ceram. Soc. 74 (1991) 270–273.

[85] J. DiCarlo, A. Navrotsky, Energetics of cobalt (II) oxide with the Zinc-blende structure, J. Am. Ceram. Soc. 76 (1993) 2465–2467.

[86] H. Zeng, J. Lin, K. Tan, Memory effect of ZrO2 matrix on surface Co3O4–CoO transition, J. Mater. Res. 10 (1995) 3096–3105.

[87] F. Yang, X. Gao, J. Xie, X. Liu, J. Jiang, X. Lu, Cobalt-based electrocatalysts as air cathodes in rechargeable Zn–air batteries: advances and challenges, Small Struct. 2 (2021) 2100144.

[88] H. Zhong, C.A. Campos-Roldán, Y. Zhao, S. Zhang, Y. Feng, N. Alonso-Vante, Recent advances of cobalt-based electrocatalysts for oxygen electrode reactions and hydrogen evolution reaction, Catalysts 8 (2018) 559.

[89] J. Wang, W. Cui, Q. Liu, Z. Xing, A.M. Asiri, X. Sun, Recent progress in cobalt-based heterogeneous catalysts for electrochemical water splitting, Adv. Mater. 28 (2016) 215–230.

[90] J. Zhong, Y. Yu, D. Zhang, K. Ye, Merging cobalt catalysis and electrochemistry in organic synthesis, Chin. Chem. Lett. 32 (2021) 963–972.

[91] Y. Xu, W. Sun, J. Cheng, X. Yang, G. Dai, J. Liu, Enhancing hydrogenation with Co/Cu foam electrode to achieve wide-range electroreduction of nitrate to ammonia, Electrochim. Acta 472 (2023) 143348.

[92] A. Shahzad, F. Zulfiqar, M.A. Nadeem, Cobalt containing bimetallic ZIFs and their derivatives as OER electrocatalysts: a critical review, Coord. Chem. Rev. 477 (2023) 214925.

[93] S. Lu, H. Wang, J. Zhou, X. Wu, W. Qin, Atomic layer deposition of ZnO on carbon black as nanostructured anode materials for high-performance lithium-ion batteries, Nanoscale 9 (2017) 1184–1192.

[94] M.S. Ahmed, B. Choi, Y.-B. Kim, Development of highly active bifunctional electrocatalyst using Co3O4 on carbon nanotubes for oxygen reduction and oxygen evolution, Sci. Rep. 8 (2018) 2543.

[95] T. Wan, H. Wang, L. Wu, C. Wu, Z. Zhang, S. Liu, J. Fu, J. Li, Niobium-doped conductive TiO-TiO2 heterostructure supported bifunctional catalyst for efficient and stable zinc-air batteries, J. Colloid Interface Sci. 651 (2023) 27–35.
[96] S. Gupta, R. Fernandes, R. Patel, M. Spreitzer, N. Patel, A review of cobalt-based catalysts for sustainable energy and environmental applications, Appl. Catal. Gen. 661 (2023) 119254.
[97] V. Singh, T. Wu, C. Tenailleau, T. Hungria, A. Estève, C. Rossi, Investigating the reaction mechanism of zirconium as a fuel in reactive multilayer films via multimodal analysis, Chem. Eng. J. 495 (2024) 153357.
[98] H.H. Shin, L. Lu, Z. Yang, C.J. Kiely, S. McIntosh, Cobalt catalysts decorated with platinum atoms supported on barium zirconate provide enhanced activity and selectivity for CO2 methanation, Acs Catal. 6 (2016) 2811–2818.
[99] S. Kim, M.A. Mahadik, A. Periyasamy, W.-S. Chae, J. Ryu, S.H. Choi, J.S. Jang, Rational design of interface refining through Ti 4+/Zr 4+ diffusion/doping and TiO 2/ZrO 2 surface crowning of ZnFe 2 O 4 nanocorals for photoelectrochemical water splitting, Catal. Sci. Technol. 11 (2021) 3141–3152.
[100] S. Bagheri, N. Muhd Julkapli, S. Bee Abd Hamid, Titanium dioxide as a catalyst support in heterogeneous catalysis, Sci. World J. 2014 (2014) 727496.
[101] V. Paranthaman, S. pandian Muthu, P. Alagarsamy, H. nay Ming, R. Perumalsamy, Influence of zirconium dioxide and titanium dioxide binders on the photovoltaic performance of dye sensitized solar cell tungsten carbide nanorods based counter electrode, Electrochim. Acta 211 (2016) 375–384.
[102] M. Chisaka, A. Ishihara, K. Ota, H. Muramoto, Synthesis of carbon-supported titanium oxynitride nanoparticles as cathode catalyst for polymer electrolyte fuel cells, Electrochim. Acta 113 (2013) 735–740.
[103] H. Nagaoka, F. Ma, D.W. Dequilettes, S.M. Vorpahl, M.S. Glaz, A.E. Colbert, M. E. Ziffer, D.S. Ginger, Zr incorporation into TiO2 electrodes reduces hysteresis and improves performance in hybrid perovskite solar cells while increasing carrier lifetimes, J. Phys. Chem. Lett. 6 (2015) 669–675.
[104] J. Azizi, M.A. Kamyabi, Pulse-electrodeposition of PtNi nanoparticles on a novel substrate of multi-walled carbon nanotubes/poly (eriochrome blue-black B) as an active and durable catalyst for the electrocatalytic oxidation of methanol, J. Electroanal. Chem. 920 (2022) 116642.
[105] A. Baz, S.T. Dix, A. Holewinski, S. Linic, Microkinetic modeling in electrocatalysis: applications, limitations, and recommendations for reliable mechanistic insights, J. Catal. 404 (2021) 864–872.
[106] A.H. Wani, A. Sharma, Optimizing the electrocatalytic discovery with machine learning as a novel paradigm. Electrocatalytic Mater, Springer, 2024, pp. 247–269.
[107] P. Maragakis, S.A. Andreev, Y. Brumer, D.R. Reichman, E. Kaxiras, Adaptive nudged elastic band approach for transition state calculation, J. Chem. Phys. 117 (2002) 4651–4658.
[108] N. Goncharova, J. Hoja, Nudged-elastic band calculations of polymorph transitions and solid-State reactions in molecular crystals, ArXiv Prepr. ArXiv241010506 (2024).
[109] N. Humphrey, S. Bac, S.Mallikarjun Sharada, Ab initio molecular dynamics reveals new metal-binding sites in atomically dispersed Pt1/TiO2 catalysts, J. Phys. Chem. C 124 (2020) 24187–24195.
[110] M. Andersen, K. Reuter, Adsorption enthalpies for catalysis modeling through machine-learned descriptors, Acc. Chem. Res. 54 (2021) 2741–2749.
[111] A.J. Chowdhury, W. Yang, E. Walker, O. Mamun, A. Heyden, G.A. Terejanu, Prediction of adsorption energies for chemical species on metal catalyst surfaces using machine learning, J. Phys. Chem. C 122 (2018) 28142–28150.
[112] P. Liu, L. Wang, R. Ranjan, G. He, L. Zhao, A survey on active deep learning: from model driven to data driven, ACM Comput. Surv. CSUR 54 (2022) 1–34.
[113] S. Faraji, Z. Wang, P. Lopez-Rivera, M. Liu, Advancements in computational approaches for rapid metal site discovery in carbon-based materials for electrocatalysis, Energy Adv. 2 (2023) 1781–1799.
[114] H. Mai, T.C. Le, D. Chen, D.A. Winkler, R.A. Caruso, Machine learning for electrocatalyst and photocatalyst design and discovery, Chem. Rev. 122 (2022) 13478–13515.
[115] S. Jain, G. Seth, A. Paruthi, U. Soni, G. Kumar, Synthetic data augmentation for surface defect detection and classification using deep learning, J. Intell. Manuf. 33 (2022) 1007–1020.
[116] E. Kim, K. Huang, S. Jegelka, E. Olivetti, Virtual screening of inorganic materials synthesis parameters with deep learning, Npj Comput. Mater. 3 (2017) 53.
[117] C. Qin, J. Liu, S. Ma, J. Du, G. Jiang, L. Zhao, Inverse design of semiconductor materials with deep generative models, J. Mater. Chem. A 12 (2024) 22689–22702.
[118] Y. Dong, D. Li, C. Zhang, C. Wu, H. Wang, M. Xin, J. Cheng, J. Lin, Inverse design of two-dimensional graphene/h-BN hybrids by a regressional and conditional GAN, Carbon 169 (2020) 9–16.
[119] M. Harussani, S. Sapuan, U. Rashid, A. Khalina, R. Ilyas, Pyrolysis of polypropylene plastic waste into carbonaceous char: priority of plastic waste management amidst COVID-19 pandemic, Sci. Total Environ. 803 (2022) 149911.
[120] C.E. Alvarez-Pugliese, D. Donneys-Victoria, W.J. Cardona-Velez, G.G. Botte, Perspectives on electrochemical valorization of organic waste, Curr. Opin. Electrochem. 46 (2024) 101508.
[121] W. Mook, M. Aroua, G. Issabayeva, Prospective applications of renewable energy based electrochemical systems in wastewater treatment: a review, Renew. Sustain. Energy Rev. 38 (2014) 36–46.
[122] H. Liu, H. Yu, Ionic liquids for electrochemical energy storage devices applications, J. Mater. Sci. Technol. 35 (2019) 674–686.